LEVEL III

12

B.S.

EPITAXIAL GROWTH OF SEMI-INSULATING GaAs

RCA Laboratories
Princeton, New Jersey 08540

INTERIM REPORT
for the period 1 July 1978 to 31 March 1979

Sponsored by
Defense Advanced Research Projects Agency (DOD)
Arlington, Virginia 22209

DARPA Order No. 3441 BASIC
Program Code No. 7D10

Monitored by
Office of Naval Research
Arlington, Virgina 22217
Under Contract No. N00014-77-C-0542

UNCLASSIFIED

SECURITY CLASSIFICATION OF THIS PAGE (When Data Entered)

REPORT DOCUMENTATION PAGE	READ INSTRUCTIONS BEFORE COMPLETING FORM
1. REPORT NUMBER	2. GOVT ACCESSION NO.
3. RECIPIENT'S CATALOG NUMBER	
4. TITLE (and Subtitle) EPITAXIAL GROWTH OF SEMI-INSULATING GaAs.	5. TYPE OF REPORT & PERIOD COVERED Interim Report, 1 July 1978 - 31 March 1979
	6. PERFORMING ORG. REPORT NUMBER PRRL-79-CR-20
7. AUTHOR(s) S. T. Jolly, E. C. Douglas, S. G. Liu, C. P. Wu, Y. H. Yun and S. Y. Narayan	8. CONTRACT OR GRANT NUMBER(s) DARPA Order No. 3441 BASIC Program Code 7D10 N00014-77-C-0542
9. PERFORMING ORGANIZATION NAME AND ADDRESS RCA Laboratories Princeton, New Jersey 08540	10. PROGRAM ELEMENT, PROJECT, TASK AREA & WORK UNIT NUMBERS PE 61101E/Program Code 7D10/NR 243-018
11. CONTROLLING OFFICE NAME AND ADDRESS Defense Advanced Research Projects Agency (DOD) 1400 Wilson Boulevard Arlington, Virginia 22217	12. REPORT DATE May 1979 13. NUMBER OF PAGES 58
14. MONITORING AGENCY NAME & ADDRESS (if different from Controlling Office) Office of Naval Research Arlington, Virginia 22217	15. SECURITY CLASS. (of this report) Unclassified 15a. DECLASSIFICATION/DOWNGRADING SCHEDULE N/A

16. DISTRIBUTION STATEMENT (of this Report)

Approved for public release; distribution unlimited.

17. DISTRIBUTION STATEMENT (of the abstract entered in Block 20, if different from Report)

N00014-77-C-0542, DARPA Order-3441

18. SUPPLEMENTARY NOTES

ONR Scientific Officer
Telephone: (202) 696-4218

19. KEY WORDS (Continue on reverse side if necessary and identify by block number)

Semi-insulating (SI) GaAs	Ion implantation
Epitaxial growth	Laser annealing
Chromium doping	Trap measurement
Buffer layers	

20. ABSTRACT (Continue on reverse side if necessary and identify by block number)

The objectives of this program are to (1) develop techniques for the epitaxial growth of high-resistivity buffer layers on semi-insulating (SI) GaAs substrates, (2) investigate ion implantation of donors into GaAs over a range of 50 to 2000 keV, and (3) investigate the potential of laser annealing to remove lattice damage caused by ion implantation and to activate the implanted donors.

Preliminary results on growth of Cr-doped buffer layers by vapor-phase epitaxy (VPE) were described in our previous report. These Cr-doped layers were grown using the Ga/HCl/AsH_3/H_2 system. Based on these results specifications for a new semi-automatic gas-handling system were developed and the unit purchased from Crystal Specialties. Using this

DD FORM 1 JAN 73 1473

UNCLASSIFIED

SECURITY CLASSIFICATION OF THIS PAGE (When Data Entered)

299 000

20.

system, we have grown up to 5-μm-thick "undoped" buffer layers on SI GaAs substrates. Using NH_3 to getter Si from the gas stream, we have been able to grow even thicker buffer layers. The ability to grow undoped buffer layers by the addition of NH_3 to the gas stream has been described in the literature; we have, however, succeeded in growing thicker layers than that achieved previously.

Implant conditions for obtaining a 1-μm-deep, uniformly doped (^{28}Si) n-layer in SI GaAs were worked out. Several wafers were implanted at energies of 40, 120, 280, 500, and 900 keV. The implantations at 500 and 900 keV were carried out in a Van de Graaf machine. Preliminary SIMS (secondary ion mass spectroscopy) data show a uniform donor atom profile. Evaluation of high-energy multiple implanted layers by SIMS, van der Pauw, and C-V techniques is being carried out.

Annealing of GaAs using high-power pulsed lasers for removing lattice damage is being investigated. Both Nd:glass (photon energy 1.17 eV) and ruby (photon energy 1.78 eV) laser radiation are being studied. Since the photon energy of the Nd:glass laser is less than the bandgap (1.4 eV at 300 K) of GaAs, the optical absorption at the Nd:glass laser wavelength is strongly dependent upon the amount of impurities and lattice defects produced. Optical measurements show that damage-enhanced absorption at $\lambda = 1.06$ μm increase with implant dose. This enhanced absorption is greatly reduced following Nd:glass laser anneal as a result of lattice reordering. Electrical activation is greatly enhanced by laser annealing for samples implanted with doses higher than 3×10^{14} at./cm^2. Sheet carrier concentrations obtained are two to five times higher than with thermal anneal. The impurity distribution profile measured shows no redistribution up to laser energy density of 1 J/cm^2.

The photon energy of the ruby-laser radiation is higher than the GaAs bandgap and is strongly absorbed at the surface. Annealing experiments were carried out on samples implanted at 70, 100, and 200 keV with doses ranging between 1×10^{14} and 1×10^{16} at./cm^2. The laser was operated with output energy density between 0.5 and 2.3 J/cm^2 per 30-ns pulse. Sheet carrier concentration density of up to 6.25×10^{14} at./cm^2 with an activation efficiency of 20.8% was measured on high-dose implanted samples. These results are more than an order of magnitude higher than that for similar samples annealed thermally. Higher activation efficiencies (45 to 56%) and higher mobilities (830 to 1350 cm^2/V-s) were measured in samples implanted at lower dose level (1×10^{14} to 5×10^{14} at./cm^2). The sheet resistances were typically four to five times lower than that for thermally annealed samples. The lowest sheet resistance measured was 20.8 Ω/□. Ohmic contacts were obtained with AuGe/Ni/Au metallization evaporated at room temperature without alloying. SIMS measurements show that no impurity redistribution occurs for energy density of 1 J/cm^2 or less. Annealing with a laser energy density of 2.3 J/cm^2 shows significant redistribution as a result of damage-enhanced diffusion.

A minicomputer-controlled DLTS system for rapid and accurate evaluation of deep traps was set up. The key feature of our system is that the capacitance transient is acquired, digitized, and stored for data manipulation. This provides a degree of flexibility that cannot be realized with analog schemes.

PREFACE

This interim report describes research done in the Microwave Technology Center of RCA Laboratories during the period 1 July 1978 to 31 March 1979 in a program sponsored by Defense Advanced Research Projects Agency (DOD) under DARPA Order No. 3441 BASIC and monitored by the Office of Naval Research under Contract No. N00014-77-C-0542. F. Sterzer is the Center's Director; S. Y. Narayan is the Project Supervisor. S. T. Jolly carried out the research on epitaxial growth; E. C. Douglas, S. G. Liu, and C. P. Wu carried out the ion-implantation and laser annealing work; and Y. H. Yun made the trap measurements. The SIMS analyses were made by C. W. Magee.

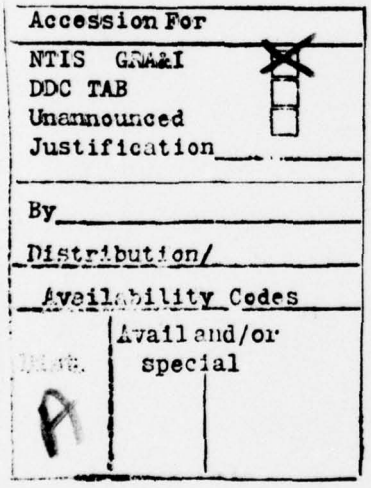

TABLE OF CONTENTS

LIST OF ILLUSTRATIONS

LIST OF ILLUSTRATIONS (Continued)

LIST OF ILLUSTRATIONS (Continued)

LIST OF TABLES

SECTION I

INTRODUCTION

The objectives of this program are to (1) develop techniques for the epitaxial growth of high-resistivity buffer layers on semi-insulating (SI) GaAs substrates, (2) investigate ion implantation of donors into GaAs over a range of 50 to 2000 keV, and (3) investigate the potential of laser annealing to remove lattice damage caused by ion implantation and to activate the implanted donors.

The preliminary results on the growth of Cr-doped buffer layers by vapor-phase epitaxy (VPE) were described in our previous report [1]. These Cr-doped layers were grown using the $Ga/HCl/AsH_3/H_2$ system. Based on these results specifications for a new semi-automatic gas-handling system were developed and the unit purchased from Crystal Specialties.* This system was received at the end of December 1978 and is being debugged. Using this system, we have grown up to 5-μm-thick 'undoped' buffer layers on SI GaAs substrates. Using NH_3 to getter Si from the gas stream, we have been able to grow even thicker buffer layers [2]. The ability to grow undoped buffer layers by the addition of NH_3 to the gas stream has been described in the literature [2]; we have, however, succeeded in growing thicker layers than that achieved previously. It is planned to grow Fe-doped buffer layers in the next program phase.

Implant conditions for obtaining a 1-μm-deep, uniformly doped (^{28}Si) n-layer in SI GaAs were worked out. Several wafers were implanted at energies of 40, 120, 280, 500, and 900 keV. The implantations at 500 and 900 keV were carried out in a Van de Graaf machine. Preliminary SIMS (secondary ion mass spectroscopy) data show a reasonably uniform donor atom profile. The evaluation of high-energy multiple implanted layers by SIMS, van der Pauw, and C-V techniques is being carried out.**

---

1. S. T. Jolly et al., Epitaxial Growth of Semi-Insulating GaAs, Annual Report, Contract N00064-77-C-0542, DARPA Order No. 3441 BASIC, Program Code 7D10, March 1978.
2. G. B. Stringfellow and G. Horn, "Hydride VPE Growth of GaAs for FETs," J. Electrochem. Soc. 124, 1806 (1977).

*Crystal Specialties, Inc., Monrovia, CA.

**Supported in part by the Office of Naval Research under Contract No. N00014-78-C-0367.

The annealing of GaAs using high-power pulsed lasers for removing lattice damage is being investigated. Both Nd:glass (photon energy 1.17 eV) and ruby (photon energy 1.78 eV) laser radiation are being studied. Since the photon energy of the Nd:glass laser is less than the bandgap (1.4 eV at 300 K) of GaAs, the optical absorption at the Nd:glass laser wavelength is strongly dependent upon the amount of impurities and lattice defects produced by implantation. Optical absorption measurements show that the damage-enhanced absorption at η = 1.06 μm increases with implant dose. This enhanced absorption is greatly reduced following Nd:glass laser anneal as a result of lattice reordering. Our results show that the electrical activation is greatly enhanced by laser annealing for samples implanted with doses higher than $3x10^{14}$at./cm^2. The sheet carrier concentration determined by van der Pauw measurement is two to five times higher than that of similar samples annealed thermally. The impurity distribution profile measured by SIMS technique shows no appreciable redistribution as a result of laser annealing up to laser energy density of 1 J/cm^2.

The photon energy of the ruby laser radiation, on the other hand, is higher than the GaAs bandgap and is thus strongly absorbed at the surface. Annealing experiments were carried out on samples implanted at 70, 100, and 200 keV with doses ranging between $1x10^{14}$ and $1x10^{16}$at./cm^2. The Q-switched ruby laser was operated with an output energy density between 0.5 and 2.3 J/cm^2 per 30-ns pulse. Sheet carrier concentration density of up to $6.25x10^{14}$at./cm^2 with an activation efficiency of 20.8% was measured on high-dose implanted samples. These results are more than an order of magnitude higher than that for similar samples annealed thermally. Higher activation efficiencies (45 to 56%) and higher mobilities (830 to 1350 cm^2/V-s) were measured in samples implanted at lower dose levels ($1x10^{14}$ to $5x10^{14}$at./cm^2). The sheet resistances were typically four to five times lower than that for thermally annealed samples. The lowest sheet resistance measured was 20.8 Ω/□. Ohmic contacts were obtained with AuGe/Ni/Au metallization evaporated at room temperature without alloying. Characteristics of ohmic contacts made to laser-annealed samples are being studied further. Forming good ohmic contacts on GaAs without alloying is obviously of great interest in device and integrated circuit fabrication. SIMS measurements show that no impurity redistribution occurs for energy density of 1 J/cm^2 or less. Annealing with a laser energy density of 2.3 J/cm^2, however, shows significant redistribution. It is believed that this is a result of damage-enhanced diffusion.

A minicomputer-controlled DLTS system for rapid and accurate evaluation of deep traps was set up. The key feature of our measurement system is that the capacitance transient is acquired, digitized, and stored for data manipulation. This provides a degree of flexibility that cannot be realized with analog schemes. Preliminary trap measurement data are presented.

SECTION II

EPITAXIAL GROWTH OF HIGH-RESISTIVITY GaAs

A. INTRODUCTION

The work described in this section is a continuation of work described in the previous report [1]. Several chromium-doped epitaxial layers and several device wafers with chromium-doped buffer layers were grown. Attempts to transport chromium using metallic chromium and a dilute mixture of chlorine in helium were unsuccessful.

During this period, the gas-feed system described in our previous report developed a number of intermittent defects (probably small leaks) which made consistent and reproducible performance of the reactor difficult. To overcome these difficulties, a new gas control system has been acquired from Crystal Specialties, Inc. This system, which is now operational, is programmable and automatically controlled; it has improved methods of gas flow control and timing. This gas system has been coupled to a 5-cm bore reactor which is capable of growing on substrates up to 3.5x3.5 cm^2. The furnace incorporates two sodium-filled heat pipes to maximize temperature uniformity and repeatability in both the deposition and reaction zones.

An arsenic trichloride vapor-phase GaAs growth system was modified to permit introduction of a dilute mixture of chromyl chloride into the gas stream. It also permits the use of other gases which may have application in the deposition of high resistance on semi-insulating GaAs.

B. NEW REACTOR SYSTEM

1. GaAs Flow Control

Gas flow rates are controlled by varying the pressure applied to pieces of stainless-steel capillary tubing whose length is chosen so that the center value of gas flow required is obtained when approximately 50 psi is applied to it. These are coupled to 0- to 100-psi pressure controllers. This system is of particular advantage when dealing with corrosive gases or with low flow rates on the order of 5 cm^3/min or less. Accurate timing of gas introduction is obtained by the use of pneumatically controlled valves which are sequenced by a programmer. The programmer outputs are preset and stored prior to a run. When repeat runs are needed, the program can be easily addressed.

2. Reactor Construction

The reactor tube assembly has been modified to give more thorough contact of the HCl to the Ga in the reactor zone. This modification prevents back-diffusion of arsenic and dopants into the gallium. Also the construction of the inlet end has been modified to reduce the possibility of leaks or diffusion of contaminants through demountable connections.

The reactor tube is surrounded by two sodium-filled heat pipes to increase temperature uniformity and repeatability. To avoid the necessity of cooling the system between runs, the furnace can be rolled away to cool the deposition zone. The reactor tube is flushed with pure N_2 from a liquid nitrogen source before introducing or removing the substrate.

C. EXPERIMENTAL RESULTS

1. Epitaxial Growth of Cr-Doped Layers

In the early part of this program phase, the effort on epitaxial growth of Cr-doped layers in reactor A [1] using CrO_2Cl_2 as the doping gas was continued. Figure 1 shows a two-point probe I-V characteristic of wafer A447. This wafer has a 5-μm-thick epitaxial layer grown on an SI GaAs substrate. The leakage current in the dark was about 2 μA at 1400 V. The top trace shows the increase in current when the sample is illuminated by a microscope lamp.

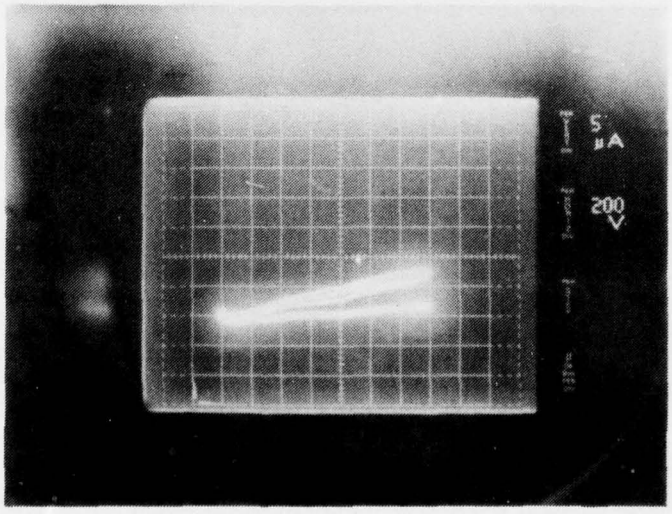

Figure 1. Two-point probe I-V characteristic of wafer A447. Top trace with illumination; bottom trace in dark.

Figure 2 shows similar traces for run A448. Figure 2(a) shows the dark and illuminated characteristic for the starting substrate while Fig. 2(b) shows similar traces after the growth of 11 μm of Cr-doped epitaxial layer.

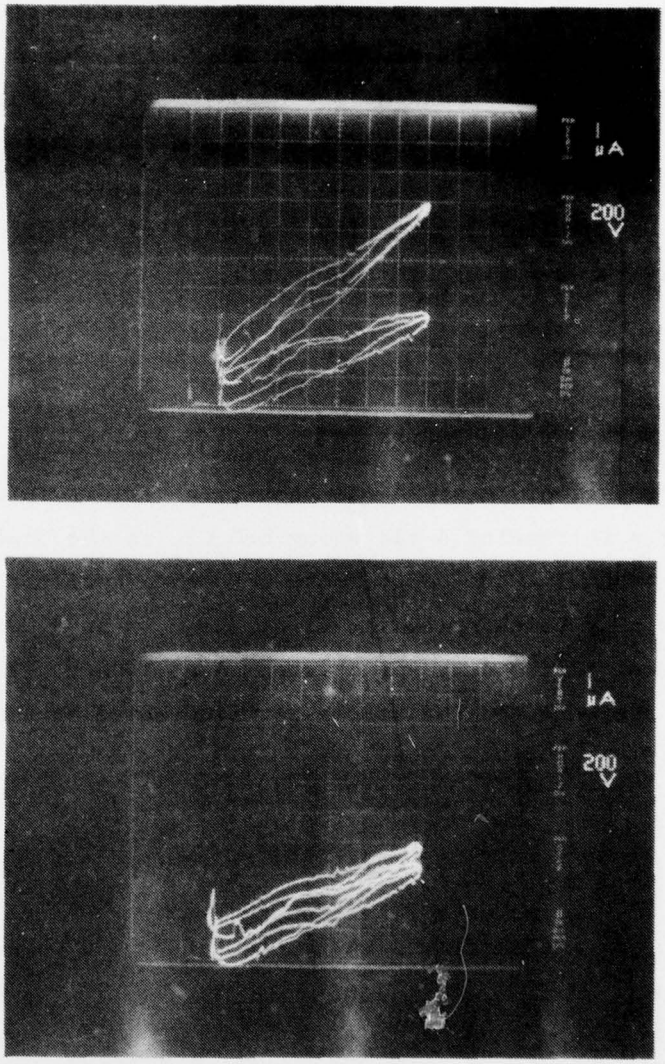

(a)

(b)

Figure 2. (a) Dark and illuminated two-point probe I-V characteristic of starting substrate. (Nikkei Kako 4418). (b) Similar characteristics of Cr-doped epitaxial layer A448.

Several thin n-type layers were grown on top of Cr-doped epitaxial buffer layers. These layers were grown in situ. Some examples are listed in Table 1.

TABLE 1. WAFERS WITH EPITAXIAL BUFFER LAYERS

Parameter	A436	A437	A441	A442
Buffer Thickness (μm)	6.5	6.0	6.0	6.0
Active Layer (μm)	1	1	1.5	1.5
Carrier Concentration (cm^{-3})	$3x10^{16}$	$1.5x10^{16}$	$4x10^{16}$	$1x10^{17}$
Room Temp Mobility	5745	6284	Not checked	Not checked
77 K ($cm^2V^{-1}s^{-1}$)	12820	15435	Not checked	Not checked

Figures 3 and 4 show the carrier concentration profiles of wafers A436 and A437, respectively, as measured by an automatic impurity profiler. Figures 5 and 6 show carrier profiles of A441 and A442 deduced from a conductivity profile assuming an average mobility.

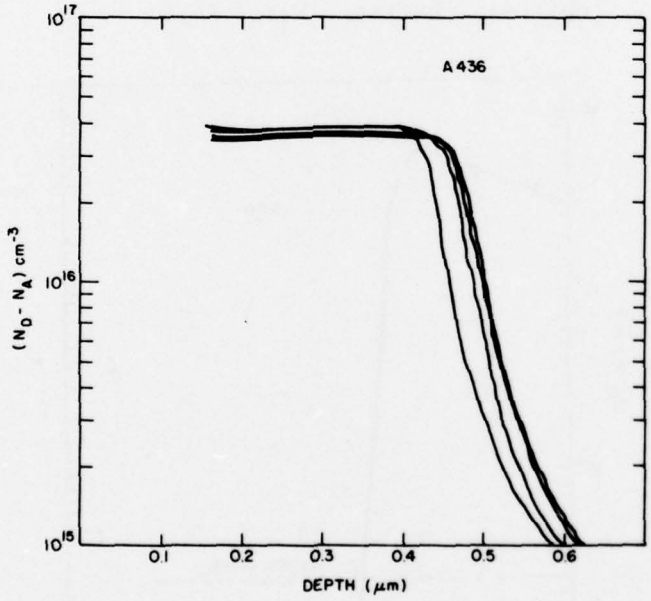

Figure 3. Carrier profile of n-layer grown on Cr-doped epitaxial buffer layer. Run A436.

As discussed in our previous report, attempts to grow n^+ layers on Cr-doped epitaxial layers were unsuccessful. The grown layers showed an anomalous diffusion of the n^+-dopant. It was suggested* that this anomalous diffusion

*M. N. Yoder, ONR, Private Communication.

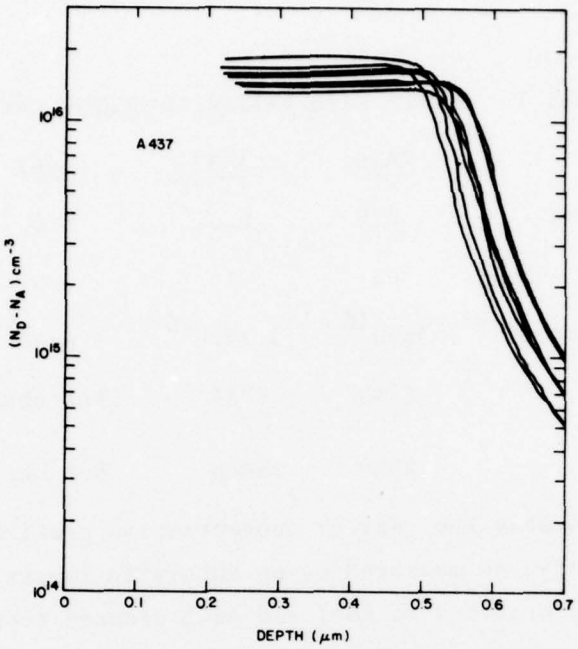

Figure 4. Carrier profile of n-layer grown on Cr-doped epitaxial buffer. Wafer A436

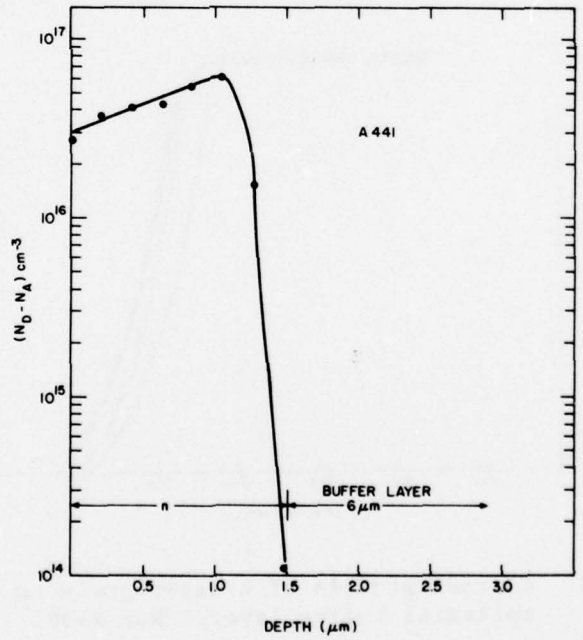

Figure 5. Carrier profile of A441 deduced from conductivity measurements assuming constant mobility.

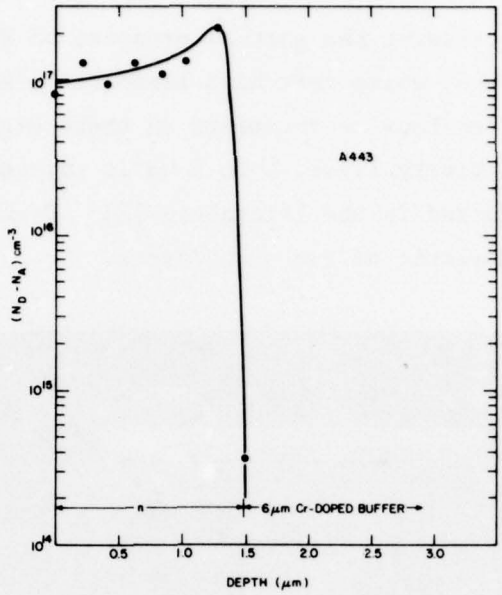

Figure 6. Carrier profile of A442 deduced from conductivity measurements assuming constant mobility.

was due to lattice damage due to excessive Cr concentration. Attempts to measure Cr concentration in epitaxial buffer layers have been unsuccessful to date. Based on these results, it was decided to attempt to reduce the background carrier concentration in the reactor so that less Cr will be required to trap the carriers and render the layer semi-insulating. It was therefore decided to implement a new reactor design.

2. Reactor B

It was decided to design, fabricate, and make operational a reactor system utilizing the Crystal Specialties gas control system, using a reactor tube and furnace assembly capable of processing a large wafer. The first task was to reduce the background carrier concentration in the reactor.

a. Gettering of Si Using NH_3

A major source of residual donors in GaAs wafers grown in a quartz reactor tube is silicon. It has been reported that the addition of NH_3 to the gas stream removes Si in the form of Si_3N_4 and prevents incorporation of Si in GaAs [2]. Under normal operating conditions, the background carrier concentration obtained in reactor B is $2\text{-}3 \times 10^{15}$ cm^{-3}. By introducing NH_3 into the gas stream, n-layers with carrier concentration on the order of 10^{13} cm^{-3} and lower

have been grown. By increasing the partial pressure of NH_3, even p-type layers have been grown. Equipment using very high impedance electrometers is being developed to allow van der Pauw measurements on these high-resistivity layers. We have grown high-resistivity layers 6 to 8 μm in thickness; this is about twice the thickness reported in the literature [2]. Figure 7 shows the two-point probe I-V characteristic of two such layers.

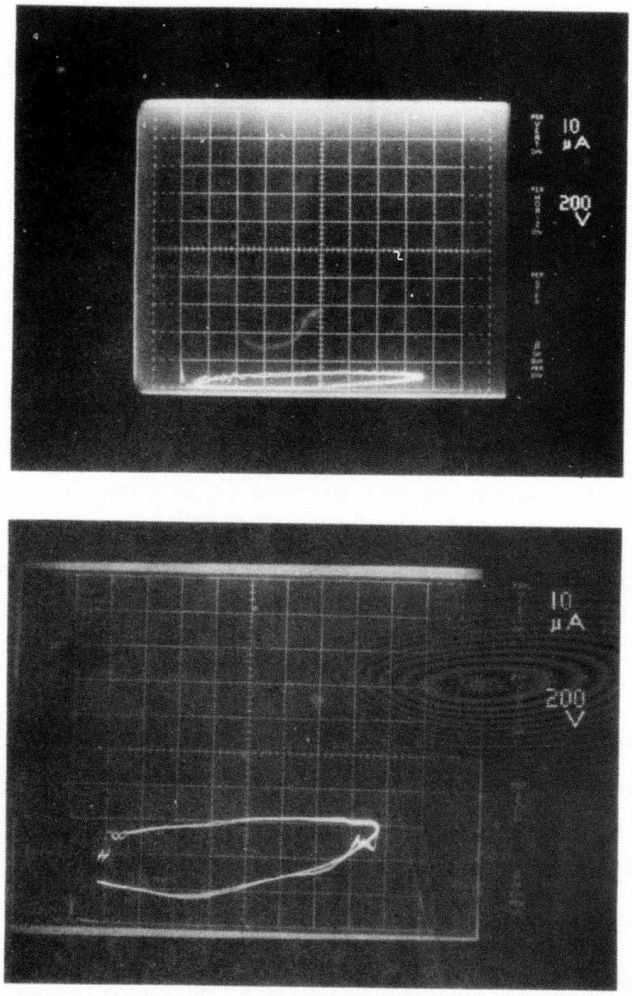

Figure 7. Two-point probe I-V characteristic of (a) B173 and (b) B233 in the dark. The wafers were grown with NH_3 in the gas stream.

The effect of the NH_3 'doped' buffer layer can be seen by the comparison of results obtained in runs B176 and B179. Run B176 is a 3.9-μm undoped layer grown on 5.5-μm-thick NH_3 'doped' buffer layer. Run B179 is a 5.5-μm-thick undoped layer. The top 2.5 μm of B179 is an n-layer of the same carrier concentration ($3x10^{15}$ cm^{-3}) as the n-layer in B176 and the bottom 3 μm is a high-resistivity layer ('undoped buffer') due to diffusion of acceptors from the SI GaAs substrate [3]. Table 2 shows the result of a van der Pauw measurement. Figures 8 and 9 show the doping profile of these wafers. A small number of TELD and FET wafers have been grown for evaluation.

TABLE 2. VAN DER PAUW MEASUREMENT

	300 K Mobility ($cm^2V^{-1}s^{-1}$)	77 K Mobility ($cm^2V^{-1}s^{-1}$)	($N_D - N_A$) cm^{-3} From CV Data
B176	7238	64,540	$3x10^{15}$
B179	7151	43,690	$3x10^{15}$

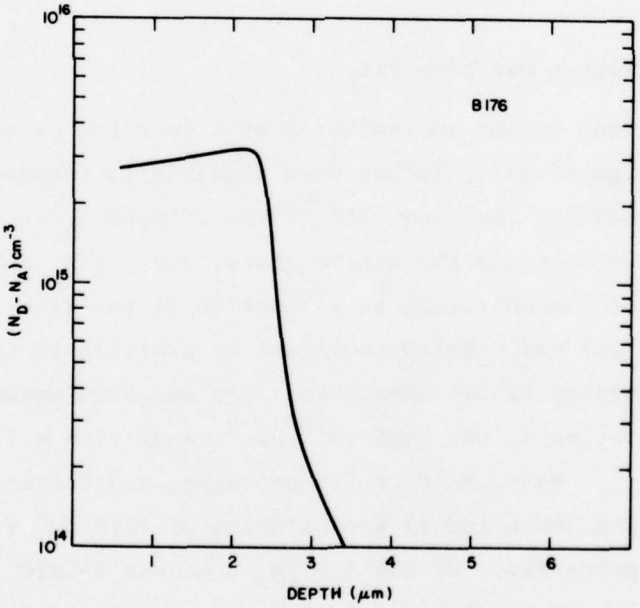

Figure 8. Carrier profile of undoped layer grown on buffer layer generated by adding NH_3 to gas stream. Buffer layer is 5.5 μm thick.

3. H. M. Cox and J. V. DiLorenco, "Characteristics of an $AsCl_3/Ga/H_2$ Two-Bubbler GaAs CVD System for MESFET Applications," Proc. Sixth Int. Symp. GaAs and Related Compounds; Inst. Phys. Conf. Series, No. 33b, London, 1977, pp. 11-22.

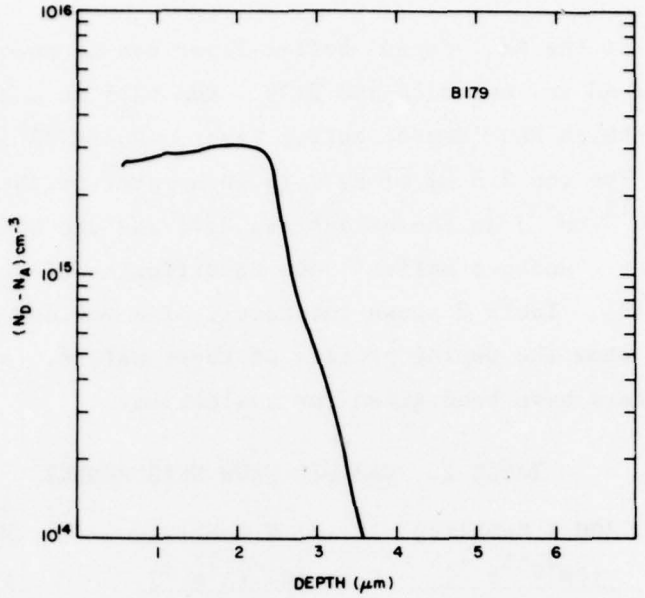

Figure 9. Carrier profile of 5.5-μm-thick undoped layer. Top 2.5 μm is $3x10^{15}$ cm^{-3} and bottom 3 μm is an 'undoped' buffer layer.

b. Effect of Carrier Gas Flow Rate

The background doping in reactor B as a function of the carrier gas flow has been investigated [4]. It has been possible to reduce the carrier concentration by reducing the flow rate of the diluent H_2 in the reactor without changing the flow rates of the active gases, viz., AsH_3 and HCl. Figure 10 shows the carrier concentration as a function of the flow rate. Wafer B287 had a thin (3.8 μm) layer which could not be profiled since the depletion layer punched through to the substrate. Van der Pauw measurements indicate a carrier concentration in the high 10^{13} cm^{-3} range with a 77 K mobility of 115,500 $cm^2V^{-1}s^{-1}$. Wafer B288, a 7.5-μm layer, had carrier concentration of $4\text{-}5x10^{14}$ cm^{-3} with 300 K and 77 K mobilities of 7786 cm^2 $V^{-1}s^{-1}$ and 114,800 cm^2 $V^{-1}s^{-1}$, respectively. Of the 7.5 μm, 3 μm was $4\text{-}5x10^{14}$ cm^{-3} and 4.5 μm was an 'undoped' buffer. Figure 11 shows the doping profile. It is planned to introduce CrO_2Cl_2 to increase the resistivity of these layers. We are also investigating potential methods of Fe doping.

4. J. K. Kennedy et al., "Effect of H_2 Carrier Gas Flow Rate on the Electrical Properties of GaAs in a Hydride System," J. Crystal Growth 24/25, 233 (1974).

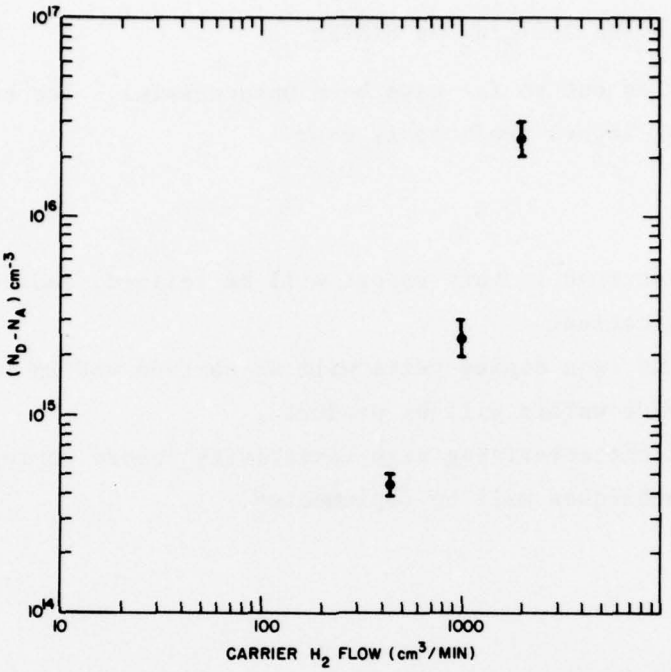

Figure 10. Effect of carrier flow rate on background effective donor concentration.

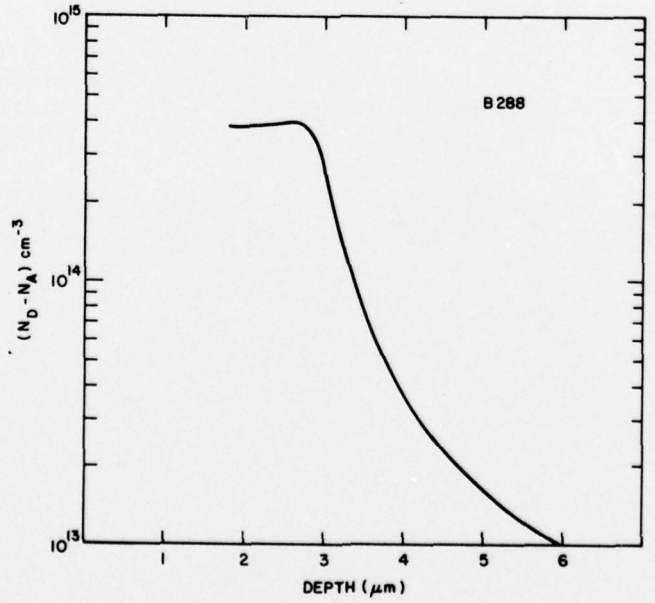

Figure 11. Carrier profile of layer grown with reduced H_2 flow. Layer thickness is 7.5 μm, 4.5 μm of which was of high resistivity.

D. Cr DOPING IN THE $AsCl_3/H_2/Ga$ SYSTEM

Tests carried out so far have been unsuccessful. The surface condition of the epitaxial layers produced is poor.

E. PLANS

Methods described in this report will be refined, and wafers will be grown for device fabrication.

Chromium and iron doping tests will be carried out in the new $AsH_3/HCl/Ga$ reactor and device wafers will be produced.

Methods of characterizing high-resistivity layers including improved van der Pauw techniques will be implemented.

SECTION III

ION IMPLANTATION

A. INTRODUCTION

One of the major reasons for the development of a technology for the epitaxial growth of SI GaAs is to use this layer as starting material for ion implantation. If high-quality, high-resistivity epitaxial layers can be repeatably grown on a variety of commercial bulk-grown SI substrates, more reproducible results can be obtained by ion implantation. We are currently investigating implantation of ^{28}Si over an energy range of 50 keV to 1.6 MeV into both commercial semi-insulating GaAs and into epitaxial buffer layers grown thereon. This implantation effort is supported in part with RCA funds and by an Office of Naval Research supported effort (N00014-78-C-0367).

B. 50- TO 250-keV IMPLANTATION

Implantation in this energy range was carried out using the machine at RCA Laboratories. The results obtained to date are described below.

1. Post-Implant Anneal

The post-implant annealing of GaAs to remove implantation damage and activate the implanted species is generally difficult since GaAs tends to dissociate at the commonly used anneal temperatures of 800 to 900°C. Dielectric encapsulation (SiO_2, Si_3N_4, AlN, etc.) has been used to prevent dissociation, but this often results in poor wafer surface due to outdiffusion of Ga or As into the encapsulant or uncontrolled indiffusion into GaAs. This is particularly detrimental to the high-quality layers required for GaAs FETs and planar Schottky varactors. We have developed a method for annealing implanted wafers without encapsulation under arsenic overpressure. This procedure has been very successful, and implanted wafers with excellent surface morphology have been obtained.

2. Carrier Concentration, Mobility, and Activation Efficiency

Implanted samples were characterized by sheet resistance and Hall measurements. Table 3 shows results obtained on S-implantation to generate n- and n^+-layers. The samples marked with a star describe implantation into epitaxial

TABLE 3. S IMPLANTATION IN GaAs

SAMPLE NUMBER	SUBSTRATE	ENERGY (keV)	DOSE (cm^{-2})	MOBILITY ($cm^2/V-s$)	APPROX. CARRIER CONC. (cm^{-3})	ACTIVATION EFF (%)
62B	SI (MM-G103)	200	4.0×10^{12}	3318	8.4×10^{16}	41.8
63B	Cr-n^-/SI* (A-141)	200	5.0×10^{12}	4053	1.8×10^{17}	72.4
10A	SI (LD)	200	5.0×10^{12}	3220	1.8×10^{17}	73.6
10D	(5-μm)n^-/SI*	200	5.0×10^{12}	4005	1.7×10^{17}	67.2
45A	(3-μm)n^-/SI* (C265)	250	7.0×10^{12}	4364	1.4×10^{17}	40.9
45E	SI (MX)	250	7.0×10^{12}	4067	1.5×10^{17}	46.9
45F	(10-μm)Cr-n^-/SI* (A90)	250	7.0×10^{12}	4331	1.2×10^{17}	37.1
19X	SI (LD)	200	7.0×10^{13}	3219	3.7×10^{17}	73.0
14C	SI (LD)	200	1.5×10^{13}	3230	2.5×10^{17}	32.8
64A	SI (MMG102)	200	2.0×10^{13}	2899	5.8×10^{17}	58.3
57	SI (XS3761)	200	1.0×10^{14}	3201	1.5×10^{18}	30.6
50A	SI (XS3761F)	200	5.0×10^{14}	2891	1.7×10^{18}	6.7

*Vapor-phase high-resistivity epitaxial layer grown on SI substrate.

buffer layers (high resistivity) grown on SI GaAs substrates. In general, implantation into epitaxial-buffer layers leads to more consistency and superior mobility for a given carrier concentration. When the substrate is of good quality (sample 45E), results comparable to implantation into epitaxial-buffers are obtained.

Figure 12 is a plot of the 300 K electron mobility of a number of implant runs. Theoretical curves for various compensation factors are also shown. Figure 13 is a plot of the average carrier concentration as a function of implant dose. Note the saturation at higher dose levels. All implants were annealed without encapsulation under arsenic overpressure at 825°C for 20 minutes. The surface morphology of annealed wafers was excellent.

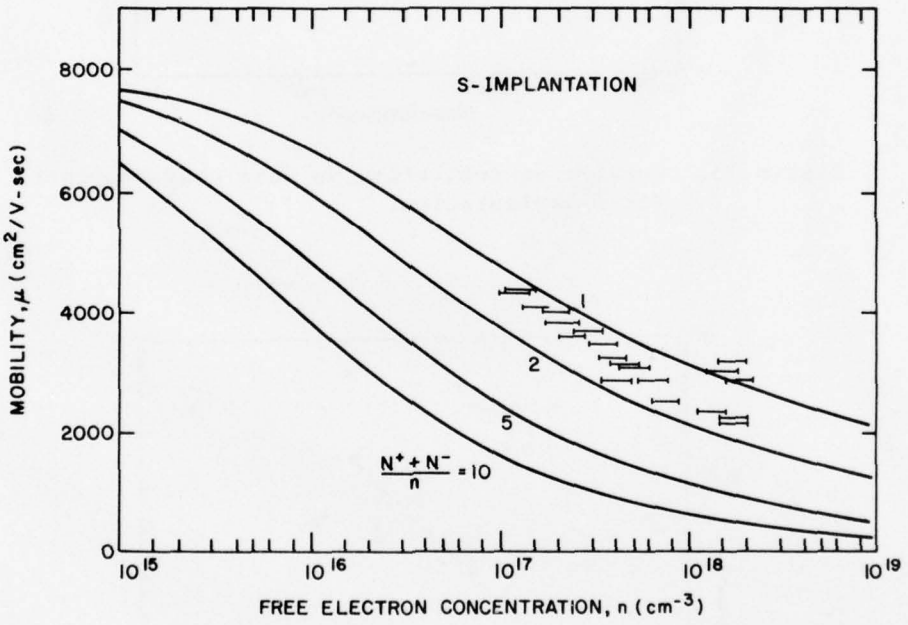

Figure 12. Mobility vs $(N_D - N_A)$ for S implantation.

Table 4 summarizes the implantation of ^{28}Si into GaAs, using the same format as in Table 3, and basically the same conclusions apply. The major difference between implantation of S and Si is that Si-implanted layers are more reproducible and follow LSS theory more closely. Figure 14 shows the carrier density-implant dose curve for Si-implantation. The data point indicated by the unfilled circle was annealed at 1000°C. The remaining data points correspond to annealing at 825°C. The anneal time was 20 minutes in all cases.

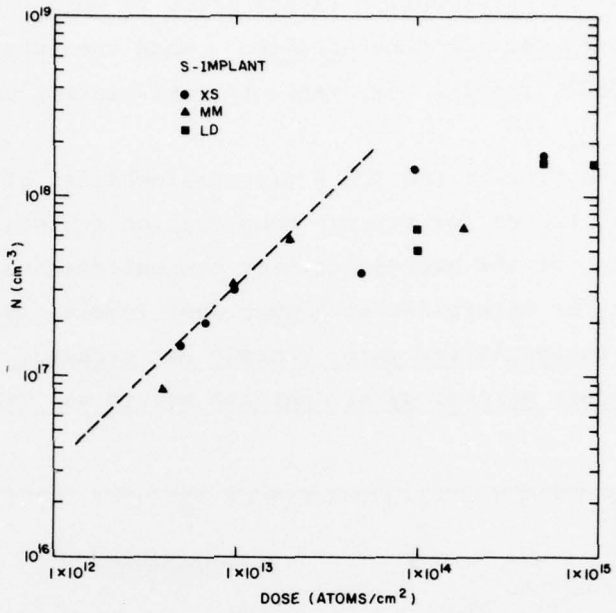

Figure 13. Carrier concentration vs dose characteristic for S implantation.

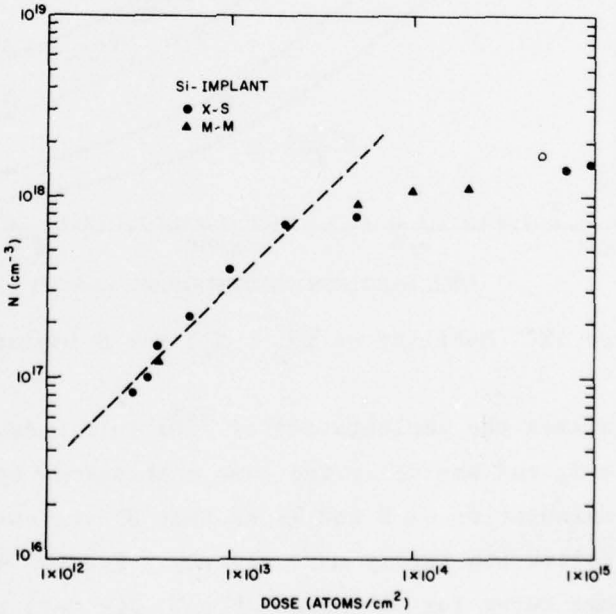

Figure 14. Carrier concentration vs dose characteristic for Si implantation.

TABLE 4. Si IMPLANTATION IN GaAs

SAMPLE NUMBER	SUBSTRATE	ENERGY (keV)	DOSE (cm^{-2})	MOBILITY ($cm^2/V\text{-}s$)	APPROX. CARRIER CONC. (cm^{-3})	ACTIVATION EFF. (%)
A24A	6-μmn$^-$/SI* (D95)	200	3.0×10^{12}	4285	8.2×10^{16}	54.9
A35A	SI (XS3761)	200	3.0×10^{12}	3374	1.9×10^{17}	82.6
		70	1.5×10^{12}			
A35C	SI (XS3765F)	200	3.0×10^{12}	3630	1.7×10^{17}	76.8
		70	1.5×10^{12}			
A35D	5-μmn$^-$/SI* (D143)	200	3.0×10^{12}	4000	1.9×10^{17}	85.1
		70	1.5×10^{12}			
A28N	SI (XS3761F)	200	3.5×10^{12}	3740	1.6×10^{17}	90.3
A23A	Cr-n$^-$/SI* (A156)	200	4.0×10^{12}	3928	1.2×10^{17}	60.5
A3A	SI (MMG102)	200	4.0×10^{12}	3570	1.2×10^{17}	62.0
A26	SI (XS3765)	200	4.0×10^{12}	4000	1.5×10^{17}	60.5
		50	2.0×10^{12}			
A4B	SI (XS3761)	200	6.0×10^{12}	3222	1.9×10^{17}	64.7
A31	SI (XS3761)	200	2.0×10^{13}	2931	7.0×10^{17}	70.1
A6	SI (MMG102)	200	5.0×10^{13}	2049	1.1×10^{18}	37.0
A34	SI (XS3761F	200	1.0×10^{14}	2204	1.1×10^{18}	21.5
A44	SI (XS3761F)	70	1.0×10^{15}	1770	1.6×10^{18}	3.2

*Vapor-phase high-resistivity epitaxial layer grown on SI substrate.

3. Carrier-Concentration Profile

Figure 15 shows the carrier concentration density profile of a Si- implanted sample as measured on automatic C-V impurity profile equipment. The implantation dose and energy level are 3.5×10^{12} at./cm^2 and 200 keV, respectively. The distribution is nearly Gaussian with a peak occurring at a depth of 0.17 μm below the surface and a standard deviation of about 0.07 μm. Figure 16 shows the profile of a multiple Si-implanted sample obtained from C-V measurement. The doping density toward the surface was increased by the low-energy implantation to result in a nearly constant carrier concentration distribution.

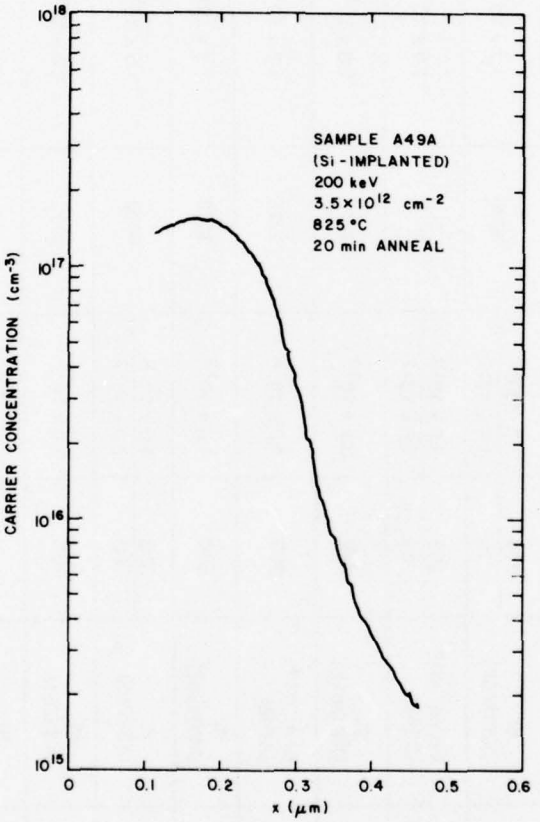

Figure 15. Carrier profile for single-energy Si implant.

4. Contact Resistivity Measurement

Contact resistivity of ohmic contacts made onto GaAs has been reported to be inversely proportional to the carrier density of GaAs. The contact resistivities of Au-Ge ohmic contacts on ion-implanted GaAs with different dose levels were studied by use of the TLM technique. Contact resistivity of 8×10^{-7} Ω-cm^2 was measured on heavily implanted samples, and $2\text{-}5 \times 10^{-5}$ Ω-cm^2 on

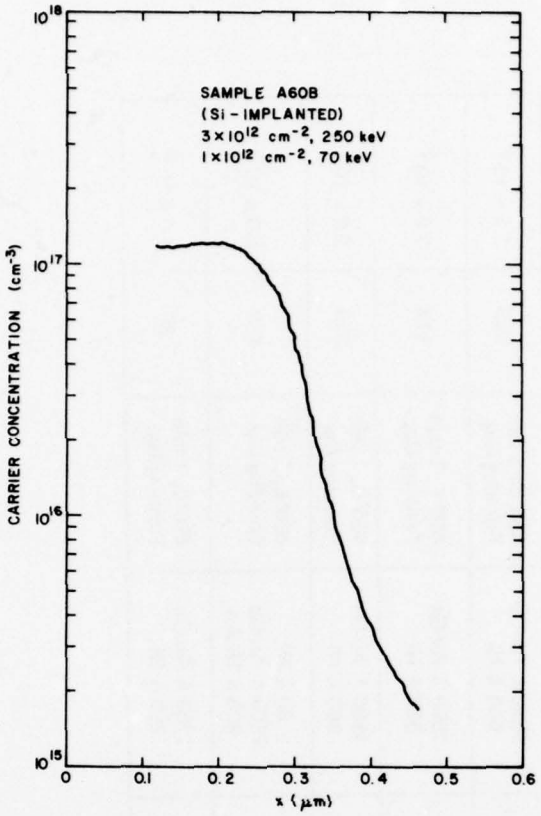

Figure 16. Carrier profile for dual Si implant.

lightly implanted samples. The carrier concentrations of the high- and low-dose samples were 1-2x10^{18}/cm^3 and 1-2x10^{17}/cm^3, respectively. The much lower contact resistivity of heavily implanted samples indicates that selective implantation can be applied in the device processing to minimize contact resistance. Results of measured contact resisitivity and sheet resistance on a number of sulfur- and silicon-implanted GaAs samples are shown in Table 5.

C. HIGH-ENERGY IMPLANTATION

High-energy (>500 keV) implantation of $^{28}Si^+$ into semi-insulating GaAs substrates was performed using a 3-MeV (max) Van de Graaf implanter equipped with a cold cathode discharge ion source. This machine is located at the Fusion Energy Corporation, Princeton, NJ. Three batches of samples were implanted. Initial results being analyzed are very encouraging.

TABLE 5. SHEET RESISTIVITY AND SPECIFIC CONTACT RESISTANCE

SAMPLE	IMPLANTED ION	DOSAGE (cm^{-2})	ENERGY (keV)	METAL CONTACT	SiNTER CONDITION	ρ_s ($\Omega/\square$)	ρ_c (Ω-cm^{-2})
A28D	Si	3.5×10^{12}	200	1500 Å Au-Ge 500 Å Ni	450°C, 1 min Forming Gas	514	3.9×10^{-5}
A35B	Si	3.0×10^{12} 1.5×10^{12}	200 70	1500 Å Au-Ge 500 Å Ni	450°C, 1 min Forming Gas	589	1.2×10^{-5}
A29	Si	5.0×10^{14} 2.0×10^{14}	200 70	1500 Å Au-Ge 500 Å Ni	450°C, 1 min Forming Gas	114	7.8×10^{-7}
5A	S	3.0×10^{13}	200	1500 Å Au-Ge 500 Å Ni	450°C, 1 min Forming Gas	259	2.4×10^{-5}
10D	S	5.0×10^{12}	200	60 Å Ni 1500 Å Au-Ge 600 Å Ni-Au	450°C, 1 min Forming Gas	432	6.0×10^{-5}
47A	S	1×10^{15}	250	750 Å Au-Ge 250 Å Ni	450°C, 1 min Forming Gas	89	4.0×10^{-6}

1. Implantation Conditions

The first batch of samples was high-dose ($\sim 3 \times 10^{15}$ at./cm^2) implanted at energy levels from 600 keV to 1.2 MeV; the second batch was implanted at 1 MeV with doses varying from 1.5×10^{13} to 5.0×10^{15} at./cm^2; and the third batch was of multiple implantations at several energy levels in an attempt to obtain a 1-μm flat profile. The implant conditions were worked out for forming 1-μm-deep Si-doped layers in GaAs with nearly constant doping throughout the layer.

Five implants ranging from 40 to 900 keV are used to construct this layer. A calculated plot of the expected doping profile is shown in Fig. 17 using a linear ordinate scale and in Fig. 18 using a log ordinate scale. Figure 19 shows plots of R_p and ΔR_p obtained either experimentally from SIMS measurements on implanted wafers or calculated using the Gibbons and Johnson implementation of the LSS theory and the electron stopping power data of Northcliffe and Schilling. At this time, the calculated R_p and ΔR_p values do not agree very well with experimental data. We therefore used extrapolated experimental curves for the determination of implant parameters to obtain a flat profile. Table 6 summarizes the implant conditions.

2. Evaluation of Implanted Wafers

The implanted GaAs wafers are being analyzed by SIMS, van der Pauw measurements, and differential C-V measurement. Figure 20 shows the SIMS profiles of the high-dose, single implantation. The profiles clearly show the depth dependence of Si atoms introduced into GaAs on the energies used. The projected ranges are, however, higher than those computed as indicated in Fig. 19. Following thermal annealing at 825°C for 20 min, sheet resistance and Hall measurements of the high-dose (3×10^{15} at./cm^2) implanted samples show that the mobilities vary between 1500 and 2200 cm^2/V-s and the sheet resistances lie between 44 and 110 Ω/□. After thermal annealing at 970°C for 20 min, sheet resistances of 27 and 22 Ω/□ with corresponding mobilities of 1500 and 1320 cm^2/V-s were measured. These results are comparable or better than those achieved with low-energy implantation. The samples were encapsulated with 2000-Å-thick sputtered Si_3N_4 during thermal annealing in a N_2 atmosphere. Figure 21 summarizes these results on high-energy single implants being evaluated to date.

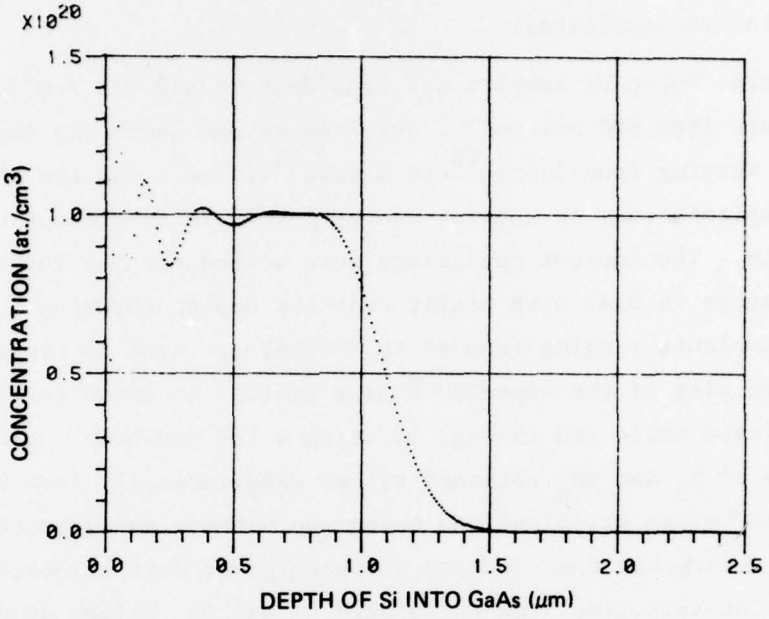

Figure 17. Computed multi-implant doping profile - linear ordinate scale.

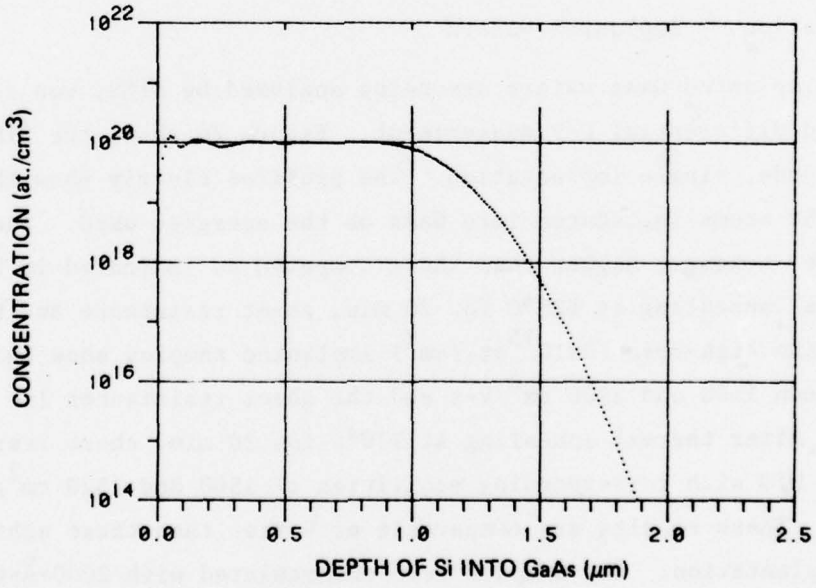

Figure 18. Computed multi-implant doping profile - log ordinate scale.

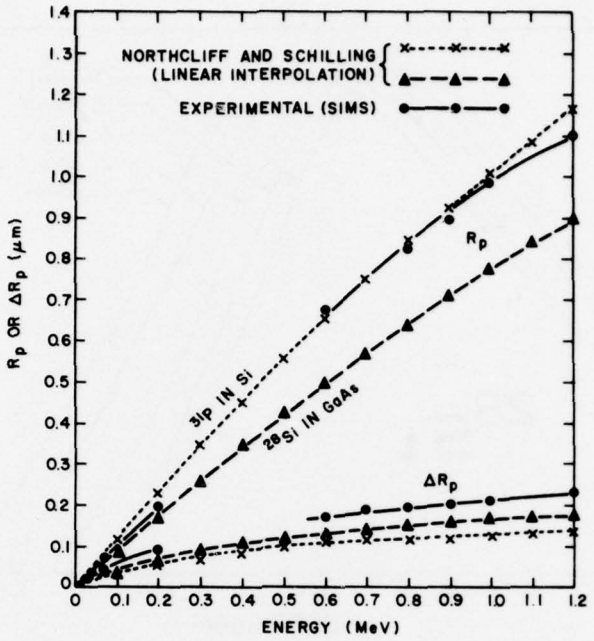

Figure 19. R_p and ΔR_p for ^{28}Si in GaAs. (Experimental values measured from SIMS profiles of actual implants. ΔR_p = full width at 0.607 x N_{max}.)

TABLE 6. IMPLANT CONDITIONS FOR FLAT PROFILE OF Si IN GaAs

Energy (keV)	40	120	280	500	900
R_p (μm)	0.0466	0.1375	0.3195	0.5500	0.8860
ΔR_p (μm)	0.0199	0.0600	0.1050	0.1500	0.1900
N_{max} (cm^{-2})	9.47×10^{19}	9.08×10^{19}	7.23×10^{19}	7.26×10^{19}	9.09×10^{19}
N_{dose} (cm^{-2})	4.70×10^{14}	1.35×10^{15}	1.9×10^{15}	2.73×10^{15}	4.33×10^{15}
Dose No.	303.6	872.0	1227	550.2	872.6
Scale	6E-6	6E-6	6E-6	6E-6	6E-6
	Area = 24.19 cm^2 (Labs machine)			Area = 7.56 cm^2 (FEC machine)	

Total Dose = $1.08 \times 10^{16}/cm^2$

Conc. Level = $1.00 \times 10^{20}/cm^3$

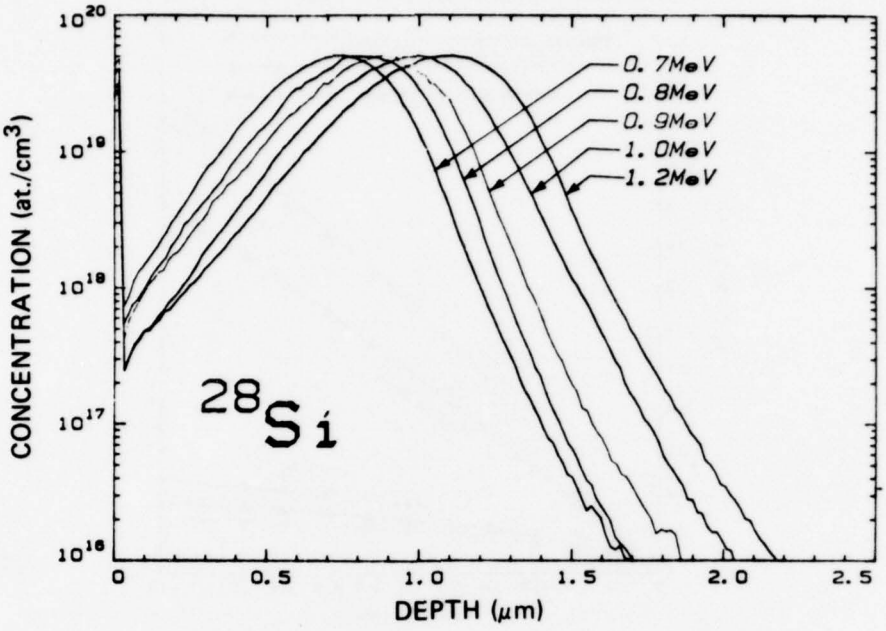

Figure 20. SIMS profile of high-dose single implants.

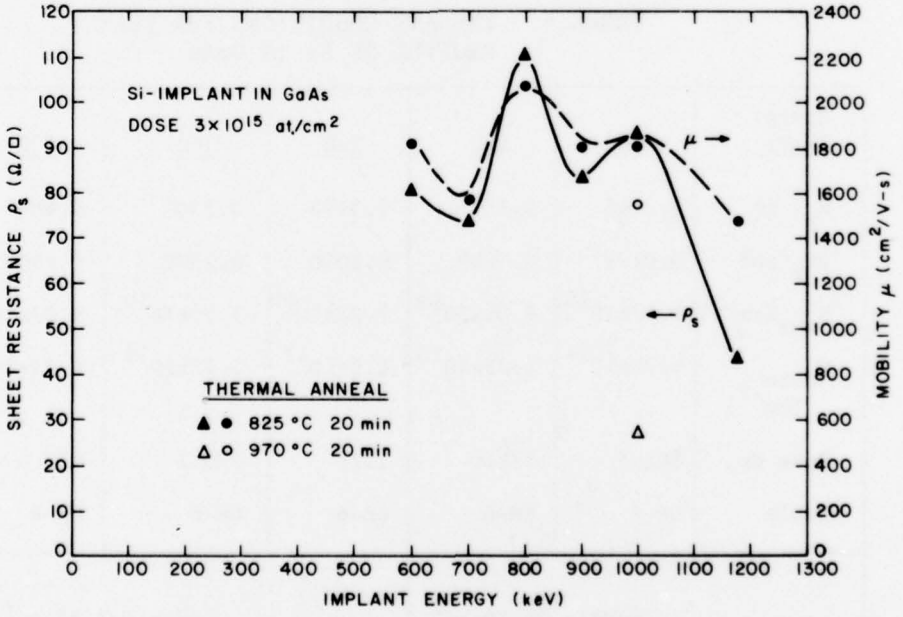

Figure 21. Mobility and sheet resistance measured after thermal annealing for samples implanted at high-energy levels.

A differential C-V technique was used in evaluation of electron density profiles of low-dose, high-energy implanted samples. This technique consists of a combination of C-V measurements and controlled layer removal by chemical etching. Figure 22 shows the depth distribution of carrier concentration measured using this technique. The circular points are normalized data from SIMS measurement on a high-dose, single-implanted (600 keV) unannealed sample. The double-hump behavior is a result of lack of an implantation in the middle (300 to 500 keV) energy region. Sheet carrier concentration and Hall measurements on the sample show that the overall mobility was 3633 $cm^2/V\text{-}s$, the sheet carrier concentration was 9.2×10^{12} at./cm^2, and the activation efficiency was 27.5%. Experiments are being continued on annealing and analyzing the remaining single and multiple high-energy implanted samples.

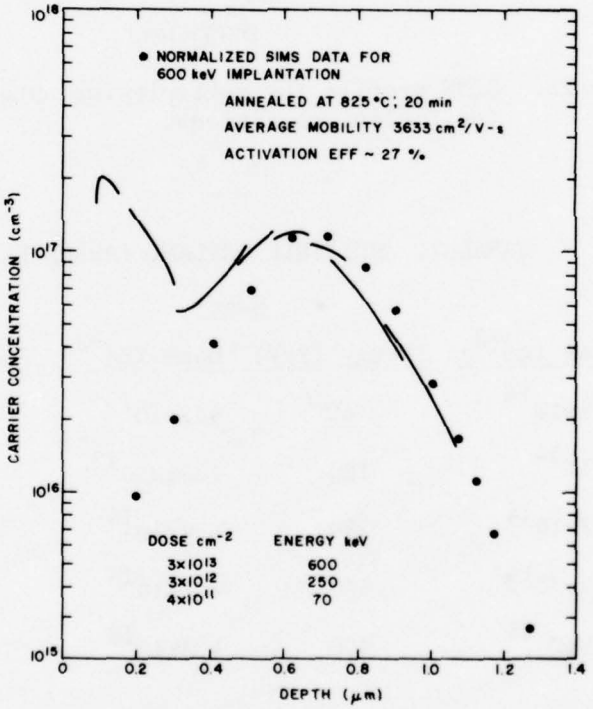

Figure 22. Composite doping profile and normalized SIMS data for multiple implantation.

Figure 23 shows the SIMS profile of high-dose multiple implanted wafers. Table 7 shows the implantation parameters for H-24, H-25, and H-28. These profiles were obtained before annealing. Note that profiles of H-24 and H-28 are in reasonable agreement with the shape of the calculated profile in Fig. 17. H-25 is much thinner than expected, and further studies are being carried out.

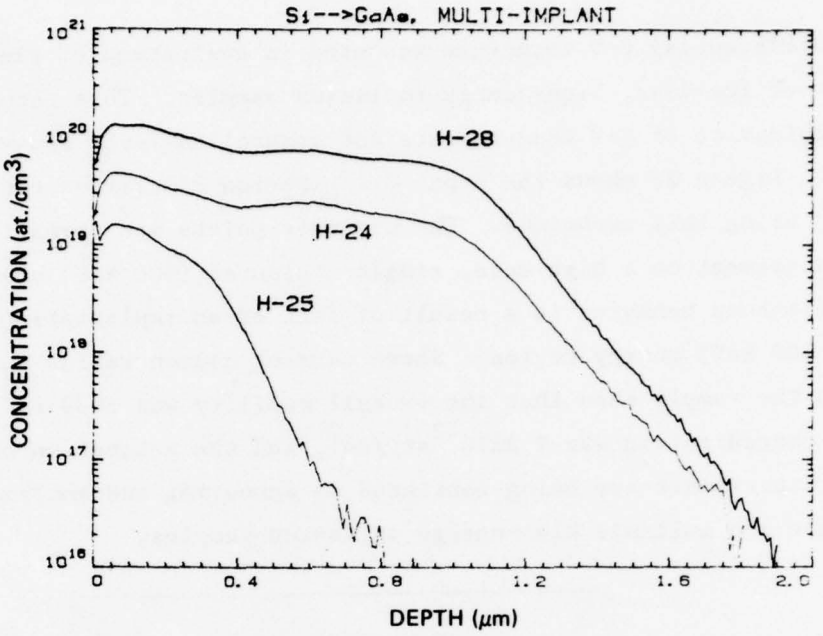

Figure 23. SIMS profile for multiple implants. See Table 7 for implant conditions.

TABLE 7. MULTIPLE IMPLANT PARAMETERS

H-24		H-25		H-28	
Energy (keV)	Dose (cm^{-2})	Energy (keV)	Dose (cm^{-2})	Energy (keV)	Dose (cm^{-2})
40	$1.4x10^{14}$	40	$4.7x10^{13}$	40	$4.7x10^{14}$
120	$4x10^{14}$	120	$1.35x10^{13}$	120	$1.35x10^{15}$
280	$5.7x10^{14}$	280	$1.9x10^{14}$	280	$1.9x10^{15}$
500	$8.2x10^{14}$	500	$2.7x10^{14}$	500	$2.7x10^{15}$
900	$1.3x10^{15}$	900	$4.3x10^{14}$	900	$4.3x10^{15}$

Figure 24 shows the SIMS profile for 1-MeV implantation at three doses. This will be used to calibrate and obtain dose-peak concentration data.

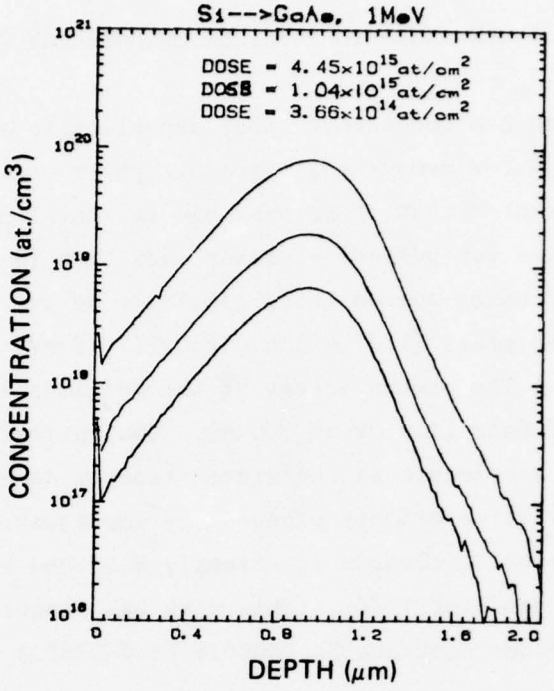

Figure 24. SIMS profile for 1-MeV implantation at three dose levels.

SECTION IV

LASER ANNEALING OF ION-IMPLANTATION GaAs

Recent research has shown that laser annealing is an attractive alternative to thermal annealing for removing lattice disorders created by ion implantation. It has been demonstrated that it is possible to anneal post-implant damage using a narrow single pulse (or pulses) of laser radiation [5-9], a scanning cw laser [10], or a scanning pulsed laser [11,12]. We are investigating the use of high-power pulsed Nd:glass (1.17 eV) and ruby (1.78 eV) laser radiation to anneal ion-implanted GaAs. The proton energy of the Nd:glass laser (1.17 eV) is less than the bandgap of GaAs (1.4 eV at 300 K). The optical absorption in GaAs at the Nd:glass laser wavelength is therefore strongly dependent upon the amount of impurities and lattice defects produced by implantation. In contrast, radiation at the ruby laser wavelength is strongly absorbed by GaAs. The results obtained to date are now described. (This work was supported in part by the Office of Naval Research under Contract No. N00016-78-C-0367.)

5. E. I. Shtyrkov, I. B. Khaibullin, M. M. Zaripov, M. F. Galyatudinov, and R. M. Bayazitov, "Local Annealing of Implantation Doped Semiconductor Layers," Sov. Phys. Semicond. 9, 1309 (1976).
6. S. U. Compisano, I. Catalano, G. Foti, E. Rimini, F. Eisen, and M. A. Nicolet, "Laser Reordering of Implanted Amorphous Layers in GaAs," Solid-State Electron. 21, 485 (1978).
7. R. T. Young, C. W. White, G. J. Clark, J. Narayan, W. H. Christie, M. Murakami, P. W. King, and S. D. Karmer, "Laser Annealing of Boron-Implanted Silicon," Appl. Phys. Lett. 32, 139 (1978).
8. S. G. Liu, C. P. Wu, and C. W. Magee, "Annealing of Ion-Implanted GaAs with Nd:Glass Laser," presented at the Symp. on Laser-Solid Interaction and Laser Proceeding (SLSILP) held in Boston, MA, Nov. 28-Dec. 1, 1978. Proceedings in press.
9. B. J. Sealy, M. H. Badawi, S. S. Kular, and K. G. Stephens, "Electrical Properties of Laser-Annealed Donor-Implanted GaAs," Electron. Lett. 14, 720 (1978).
10. A. Gat and J. F. Gibbons, "A Laser-Scanning Apparatus for Annealing of Ion-Implantation Damage in Semiconductors," Appl. Phys. Lett. 32, 142 (1978).
11. W. L. Brown, J. A. Gdovchenko, K. A. Jackson, L. C. Kimerling, H. J. Leamy, G. L. Miller, J. M. Poate, J. W. Rodgers, G. A. Rozgonyi, T. T. Sheng, T. N. C. Venkatesan, and G. K. Celler, "Laser-Annealing of Ion-Implanted Semiconductors," Proc. on Rapid Solidification Proc. - Principles and Technologies, Reston, VA, Nov. 1977.
12. R. Tsu, J. E. Baglin, G. J. Lasher, and J. C. Tsang, "Laser-Induced Damage and Recrystallization of Ion-Implanted GaAs by Frequency-Doubled Nd:Yag Laser," Presented at SLSILP (c.f. Ref. 8).

A. Nd:GLASS LASER ANNEALING

Semi-insulating GaAs substrates of (100) orientation were implanted under high vacuum with $^{28}Si^{+}$ at 70 or 200 keV and fluence between $3x10^{12}$ and $3x10^{15}$ at./cm^2. The wafers were polished on both sides and chemically etched prior to implantation. Following implantation, the 0.04-cm-thick wafer was cleaved to samples approximately 0.7x0.7 cm for laser annealing experiments. The Nd:glass laser was operated with an output energy density of between 0.2 and 2.5 J/cm^2 per pulse (25 ns). The corresponding power density lies between 8 and 100 MW/cm^2. The diameter of the laser beam is 2 cm.

Figure 25 shows comparative results of sheet carrier concentration density for Nd:glass laser and thermally annealed samples with implanted ^{28}Si doses between $3x10^{12}$ and $3x10^{15}$at./cm^2. The energy density of each laser pulse used in the annealing is indicated by crosses in the figure; it varies between 0.5 and 1.17 J/cm^2. All experiments were performed using single pulses. Figure 25 also shows that the electrical activation is greatly enhanced by laser annealing for samples implanted with doses higher than $3x10^{14}$at./cm^2. The sheet carrier concentration density N_s as determined by van der Pauw measurement is two to five times higher than that of samples thermally annealed at 825 or 1000°C for 20 min. For example, mobilities for laser-annealed samples are 253 cm^2/V-s at a sheet carrier concentration of $1.91x10^{14}$at./cm^2 and 529 cm^2/V-s at $1.25x10^{14}$ at./cm^2, compared with a mobility of 1392 cm^2/V-s at $2.9x10^{13}$at./cm^2 and 1881 cm^2/V-s at $2.8x10^{13}$at./cm^2 for similar samples annealed thermally. The low electrical activation at a lower dose level for a given pulsed laser energy may be attributed to the reduction in enhanced optical absorption. The dependence of optical absorption on the implant dose was studied by optical absorption measurements.

The optical absorption in the sample was measured by spectrophotometry. The transmission through the sample and the reflection from the sample were measured on a Cary spectrometer in the 7000- to 12,000-Å wavelength range. The absorption at a given wavelength (e.g., 1.06 μm) is calculated by the expression:

$$A = 1 - T - R$$

where A, T, and R are, respectively, absorption, transmission, and reflection which are all absolute values and are expressed in percentages. The enhanced absorption due to implantation damage is equal to $A-A_0$, where A_0 is the absorption through the unimplanted sample. At 1.06-μm wavelength, the measured value

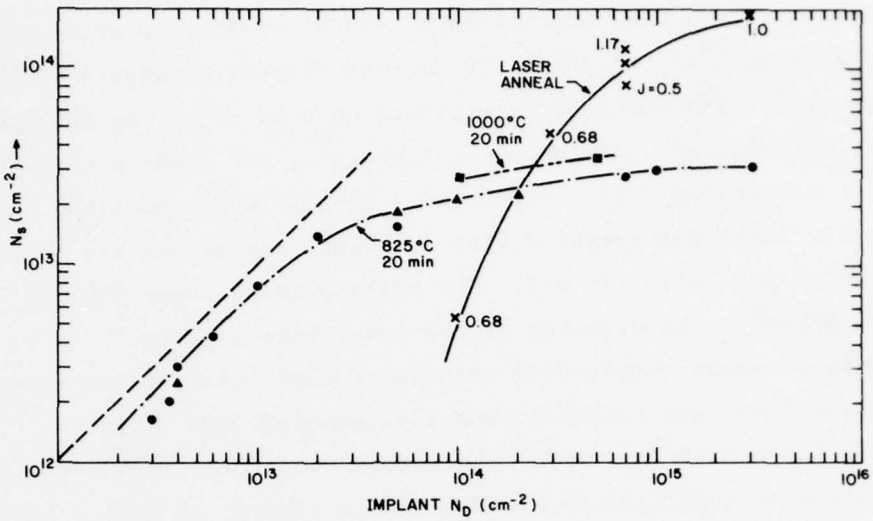

Figure 25. Comparison of thermal and laser annealing; 1.06-μm, 25-ns single-pulse (Nd:glass) laser was used.

of A_0 was typically 0.1. The reflectance was measured with reference to an aluminum mirror, and the absolute value is obtained through calibration. At 1.06 μm, the reflectance of aluminum on glass is 0.862.

Figure 26 shows the reflectance measured on an as-implanted wafer and on the same wafer laser-annealed at an energy density of 0.34 J/cm^2. Because of the enhanced absorption in the as-implanted layer, the reflection is affected only by the front (implanted) surface. Consequently, the reflectance forms a continuous line as it passes through the absorption edge as shown in Fig. 26(a). In the case of the annealed sample, restored lattice order reduces the enhanced absorption in the implanted layer. As a result, the reflectance spectrum forms a step [Fig. 26(b)] as the optical wavelength passes through the band edge of GaAs, because the reflection is greatly enhanced in the long-wavelength range due to multiple reflection from the polished sample back surface.

The transmittance through an ion-implanted sample before and after annealing is shown in Fig. 27. The gradual increase in absorption from the long-wavelength side toward the absorption edge in the as-implanted sample is a band-tailing effect produced by impurities. The transmittance at 1.06-μm wavelength changes from 0.170 for the as-implanted sample to 0.457 after laser annealing at 0.68 J/cm^2. The enhanced absorption ($A - A_0$) can be evaluated from the expression

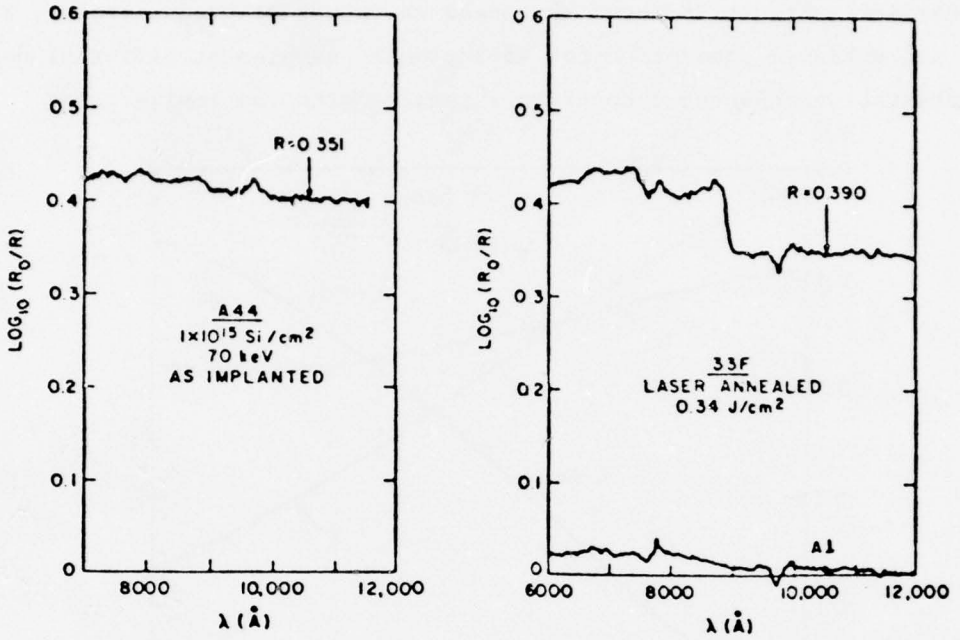

Figure 26. Optical reflection from (a) as-implanted sample and (b) same sample following laser annealing.

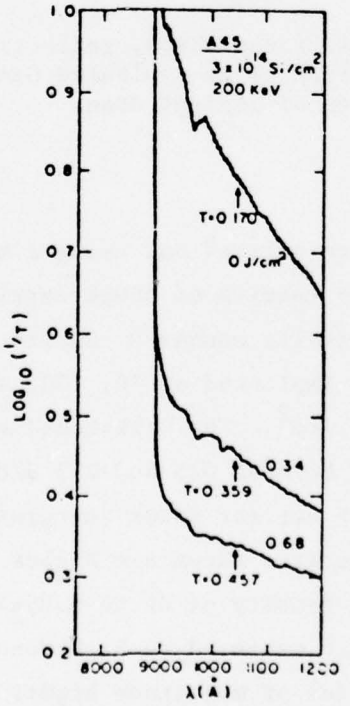

Figure 27. Optical transmission from Si-implanted GaAs sample annealed at different laser energy density.

given earlier. Figure 28 shows the measured values of transmittance, reflectance, and enhanced absorption for as-implanted samples at different dose levels. The implantation-enhanced absorption increases with the implant dose.

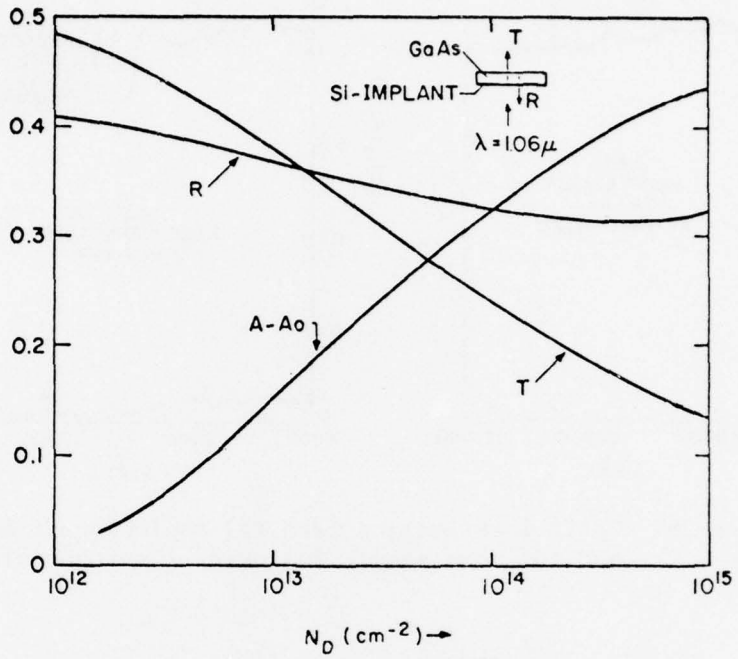

Figure 28. Optical transmission, reflection, and enhanced absorption of as-implanted GaAs samples as a function of implant dose.

B. RUBY-LASER ANNEALING

Similar experiments were carried out using a high-power pulsed (30 ns) ruby laser. Figure 29 shows results of sheet carrier concentration density for ruby-laser annealed and thermally annealed samples. Laser annealing experiments were carried out on samples implanted at 70, 100, and 200 keV with doses ranging between $1x10^{14}$ and $1x10^{16}$ at./cm^2. The Q-switched ruby laser was operated with an output energy density of between 0.5 and 2.3 J/cm^2 per 30-ns pulse. The data points shown in Fig. 29 are for laser energies of 1.7 and 2.3 J/cm^2. It should be noted that the energies shown are higher than those shown in Fig. 25. Sheet carrier concentration density of up to $6.25x10^{14}$ at./cm^2 with an activation efficiency of 20.8% were measured on high-dose implanted samples. These results are more than an order of magnitude higher than those for similar samples annealed thermally. Higher activation efficiencies (45 to 56%) and higher

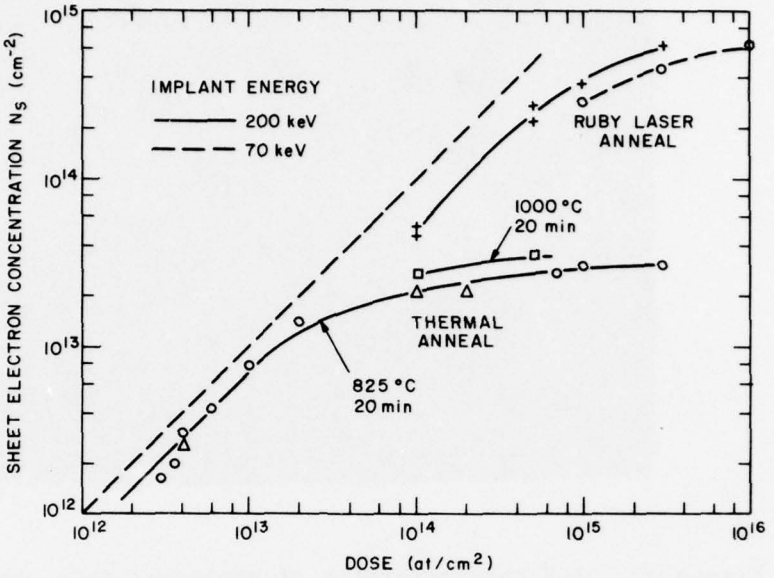

Figure 29. Dose-sheet electron concentration for ruby laser and thermal anneal.

mobilities (830 to 1350 cm^2/V-s) were measured in samples implanted at lower dose levels ($1x10^{14}$ to $5x10^{14}$ at./cm^2). The sheet resistances were typically four to five times lower than those for thermally annealed samples. The lowest sheet resistance measured was 20.8 Ω/□. Ohmic contacts were obtained with AuGe/Ni/Au metallization evaporated at room temperature without alloying. Figure 30 shows the I-V characteristics between unalloyed ohmic contacts. Characteristics of ohmic contacts made to laser-annealed samples are being studied further. Forming good ohmic contacts on GaAs without alloying is obviously of great interest in device and integrated-circuit fabrication.

C. SIMS MEASUREMENT AND SURFACE MORPHOLOGY STUDY

Impurity distribution in as-implanted, thermal-annealed, Nd:glass laser-annealed, and ruby laser-annealed samples have been investigated with the SIMS technique. Figure 31 shows SIMS profiles of a sample before and after thermal annealing (825°C, 20 min) under As overpressure. These data show that there is no measurable impurity redistribution due to the thermal anneal procedure used. Figure 32 shows the result of a sample implanted with a dose of $1x10^{15}$ at./cm^2 at an energy level of 70 keV, before and after irradiation with a

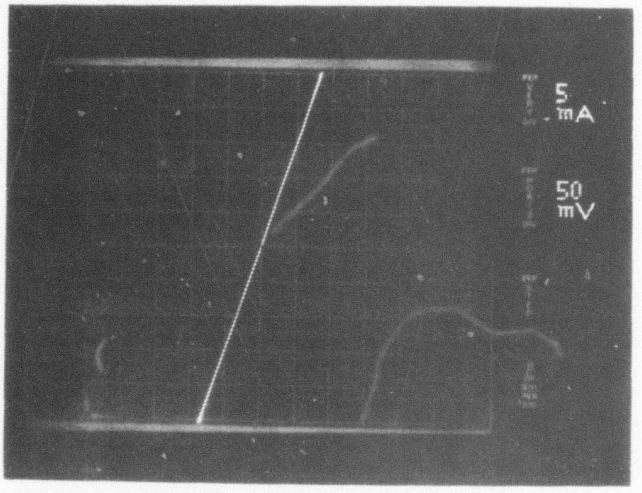

Figure 30. I-V characteristic of unalloyed AuGe ohmic contacts on laser-annealed ion-implanted GaAs.

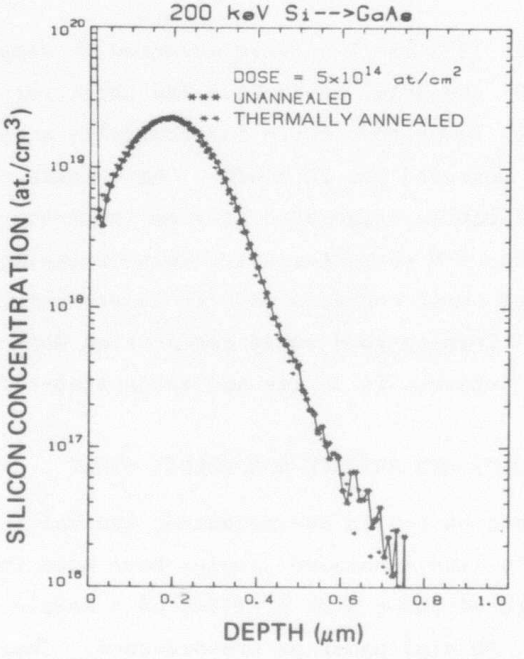

Figure 31. SIMS study of thermal annealing.

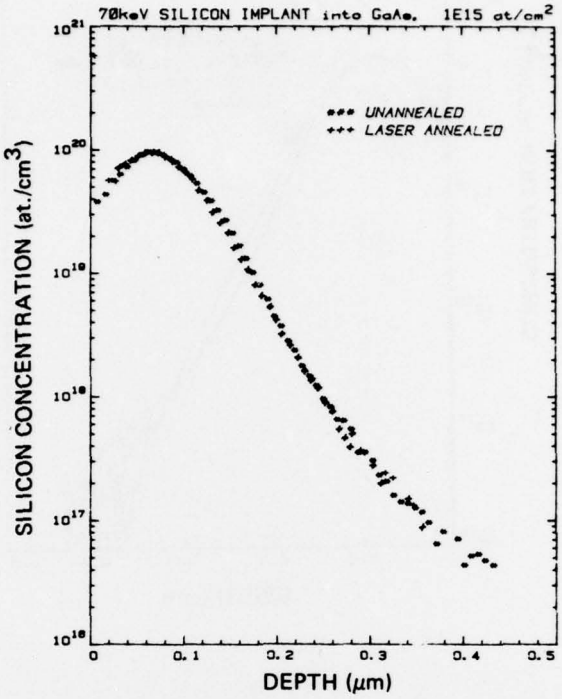

Figure 32. SIMS measurement on laser-annealed sample.

0.34-J/cm^2 Nd:glass laser pulse (25 ns). Again there is no evidence of impurity redistribution. Figure 33 shows the result of a sample implanted with a dose of 3x10^{15}at./cm^2 at an energy level of 200 keV after thermal annealing (825°C, 20 min), laser annealing with a 1.0-J/cm^2 ruby laser pulse (30 ns), and before annealing. Note again the absence of impurity redistribution.

Figure 34 shows the result of a sample implanted with a dose of 1x10^{16}at./cm^2 at an energy level of 70 keV after thermal annealing (825°C, 20 min), ruby annealing at an energy density of 2.3 J/cm^2, and before annealing. The impurity profile of the laser-annealing sample at an energy level of 2.3 J/cm^2 shows substantial broadening compared with both thermal-annealed and as-implanted samples. Note also that there is evidence of impurity redistribution in the thermally annealed sample. The anomalous shoulder broadening following laser annealing in high-dose samples is believed to be associated with damage-enhanced diffusion.

The SIMS study shows that the amount of impurity redistribution seems to depend upon the energy and dose of implantation, and the energy density of the laser beam. This result suggests that melting occurs near the surface region when high-dose samples are irradiated with a high-energy density pulse, and the substantial broadening in impurity distribution is a result of diffusion in liquid GaAs.

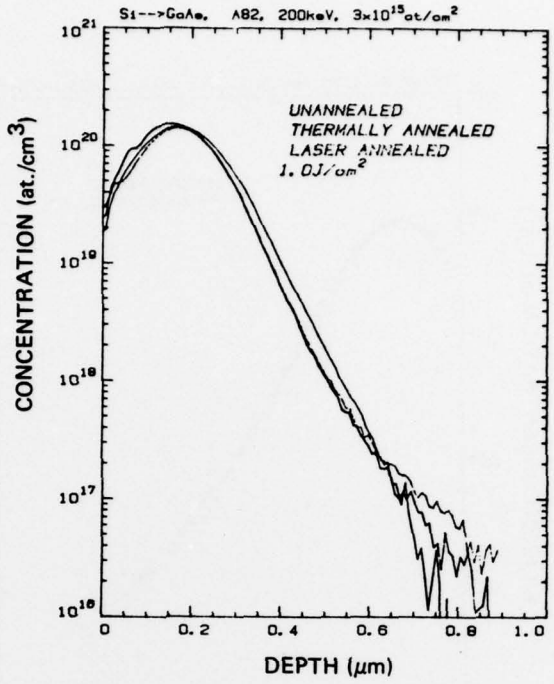

Figure 33. SIMS comparison of thermal and 1-J/cm^2 ruby-laser anneal.

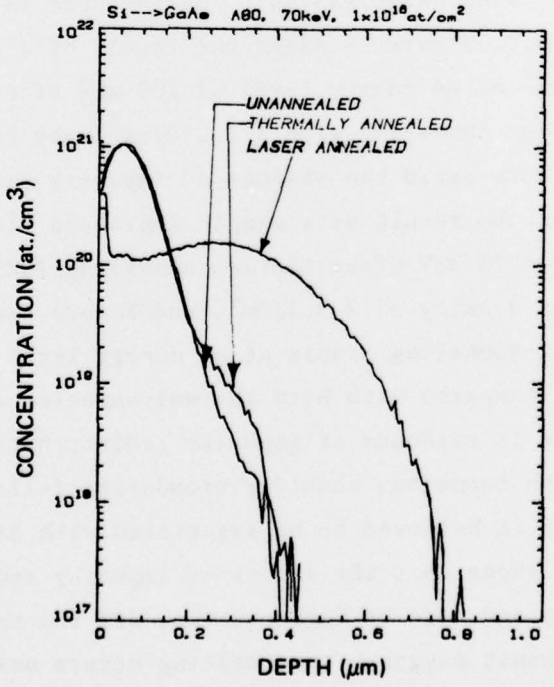

Figure 34. SIMS comparison of thermal and 2.3-J/cm^2 ruby-laser anneal.

SEM photographs of samples irradiated with a high-energy density pulse (2.3 J/cm^2) shows no detectable structures on the surface microscopically at 20K magnification, Fig. 35(b), although the sample surface appears wavy to the naked eye. A Nomarski interference contrast micrograph, Fig. 35(a), shows an uneven rippled surface. These results suggest that melting and epitaxial regrowth are associated with annealing of GaAs by high energy-density laser pulse. Similar ripples [11] were observed on laser-annealed silicon surfaces and it was suggested that the ripple formation occurs when the melting threshold is periodically exceeded. Examination of high-dose implanted GaAs samples irradiated with a laser pulse of 1-J/cm^2 SEM reveals a fine structure, Fig. 36(b), on the surface which does not appear on the as-implanted, Fig. 36(a), sample. The various observed surface conditions created by different laser energy densities are being further investigated.

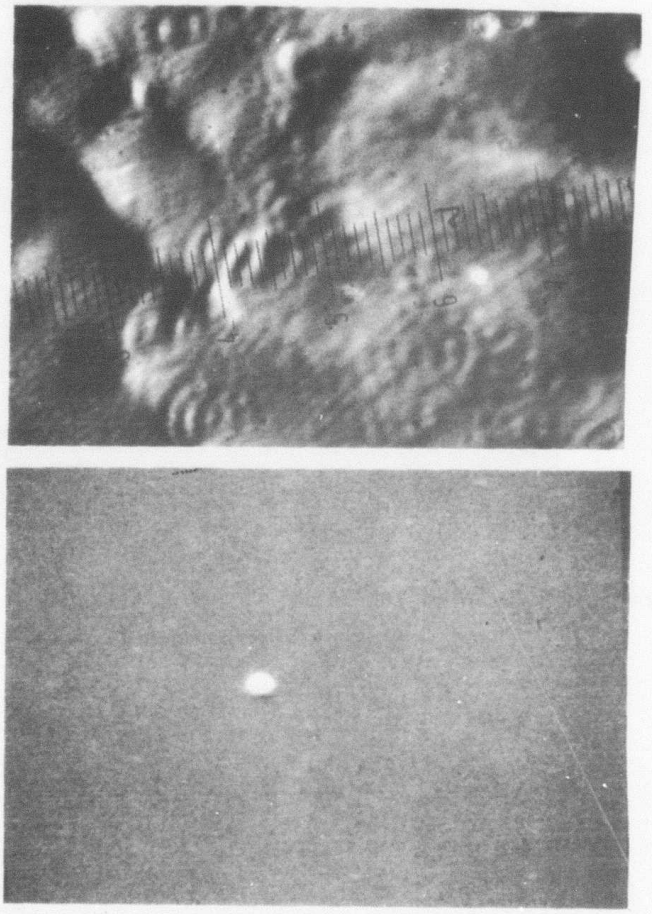

(a)

(b)

Figure 35. (a) Nomarski interference contrast. Ruby-laser anneal (2.3 J/cm^2) sample. (b) SEM of same sample at 20K magnification.

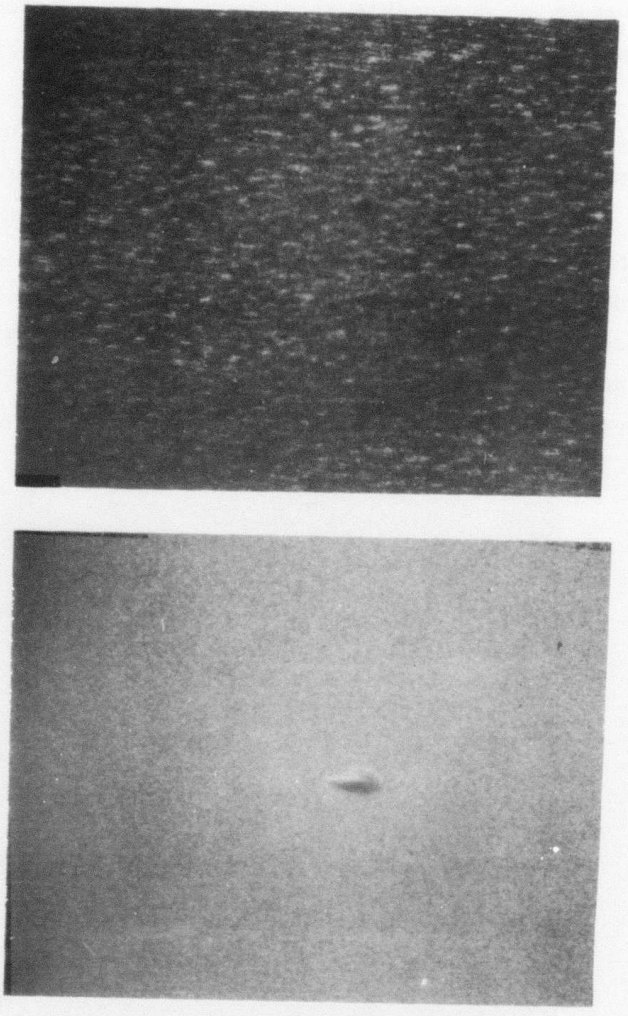

(a)

(b)

Figure 36. (a) SEM (x20K) of as-implanted sample. (b) SEM (x20K) of ruby-laser anneal (1 J/cm^2) sample.

SECTION V

TRAP MEASUREMENT

Since unwanted deep-level impurities (traps) influence the performance and reliability of GaAs devices, the detection and identification of deep-level traps are important steps toward material characterization. In ion-implanted GaAs layers on SI GaAs, traps can occur due to diffusion of deep-level impurities from the substrate, damage due to the implantation process that has not been annealed, deviations from stoichiometry caused by loss of As or Ga during annealing, etc. It is therefore desirable to measure trap energies, concentration, and their location in the ion-implanted layer. A minicomputer-controlled trap measurement system which allows a reasonably rapid and accurate determination of traps present in semiconductors is being developed.

Investigation of traps in ion-implanted and epitaxial layers was initiated in the course of the current program. One of the useful techniques for trap measurement is the recently developed [13] DLTS (deep-level transient spectroscopy) method. This trap measurement scheme basically monitors the temperature dependence of the exponential capacitance transient which results when a Schottky barrier or a p-n junction is pulsed from a slight reverse bias to a larger quiescent value, $-V_B$. The basic reverse-biased pulse sequence (V_B) and the observed capacitance signal (C) are shown in Fig. 37 for n-type material.

When the reverse-biased voltage is reduced from its quiescent value, the traps are filled by electrons. Some of the traps remain filled when the bias is abruptly returned to its initial value, $-V_B$ at time $t = 0$. The measured capacitance value is determined by the width of the depletion layer of the reverse-biased Schottky barrier or p-n junction. An increase in the depletion layer width will cause a decrease in the measured capacitance. Trapping centers in the depletion layer that are filled with electrons will cancel the contributions of an equal number of positive charges due to ionized donors in the depletion layer. More positive ionized donors must therefore be included in the depletion layer to balance the reverse bias applied to the Schottky barrier or p-n junction. The effect of trapping centers filled with electrons is to increase the depletion layer width and thereby decrease the measured capacitance

13. D. V. Lang, "Deep-Level Transient Spectroscopy: A New Method to Characterize Traps in Semiconductors," Appl. Phys. 45, 3023 (1974).

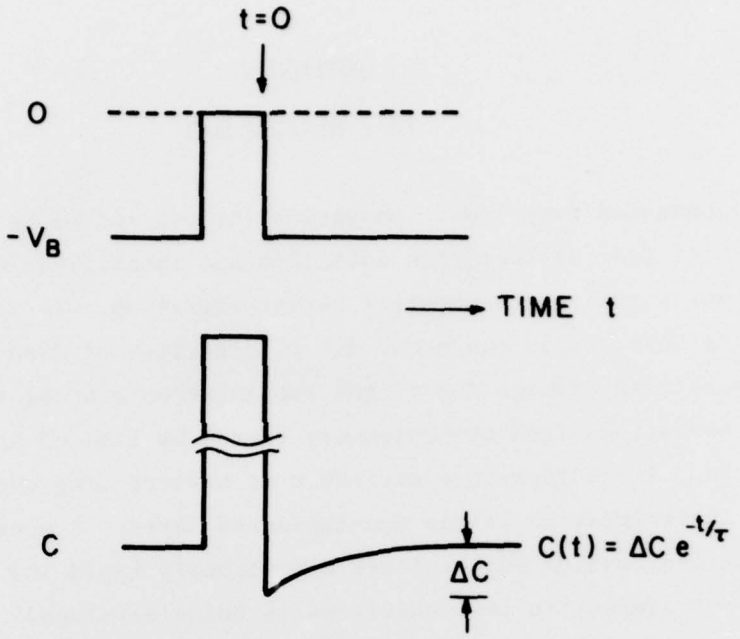

Figure 37. Basic reverse-biased pulse sequence (V_B) and the observed capacitance signal (c) as a function of time (t).

value. Thus, the capacitance value at t = 0 is slightly lower than its initial value at the bias $-V_B$. These trapped electrons have a certain probability of being thermally excited from the traps, in which case they are rapidly swept out of the depletion layer by the electric field. This leads to a reduction in the width of the depletion layer producing a corresponding exponential return of the capacitance to its initial value with a time constant τ given by:

$$\frac{1}{\tau} = \sigma_n v_{th} N_C \exp[-(E_C - E_T)/kT] \qquad (1)$$

where σ_n is the electron capture cross section, v_{th} is the thermal drift velocity of electrons, N_C is the effective density of states at the conduction band edge, k is the Boltzmann constant, and T is the absolute temperature.

The magnitude, ΔC, of the capacitance transient shown in Fig. 37 is determined by the concentration of the traps present. The time constant τ (as a function of temperature) provides information on the energy level of the traps. The slope of a plot of log τ vs 1/T indicates the trap energy level ($E_C - E_T$).

In the DLTS system under development, a Measurement and Control Processor (HP-2240)* interfaced with an RTE Minicomputer System (HP-2100)* is being used in conjunction with a capacitor bridge (PAR-410).** A block diagram of the system is shown in Fig. 38. A pulse generator (HP-214)* periodically triggers the PAR-410 capacitance bridge in a pulsed reverse-bias mode. If the sample contains deep-level traps within the depletion region, an exponential capacitance transient is detected by the PAR-410 and recorded by HP-2240. The HP-2240 is able to record a maximum of 20 readings/ms. Once the data are recorded and stored in memory, they can be processed by the RTE minicomputer using the correlation linear-filtering techniques described by G. L. Miller [14].

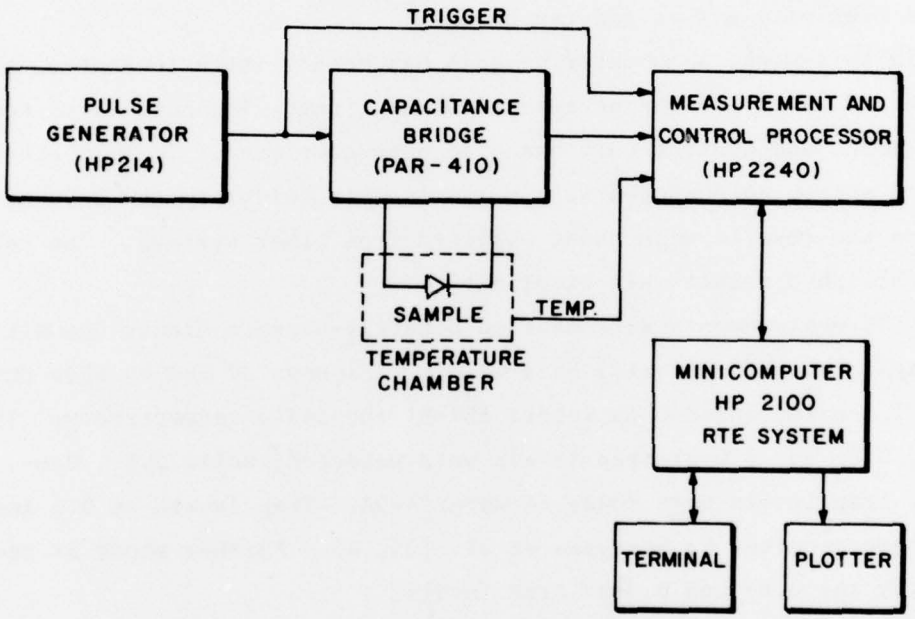

Figure 38. Block diagram of DLTS system.

The temperature of the sample is varied from 77 K up to about 450 K during each measurement. As can be seen from Eq. (1), the capacitance transient time constant τ corresponding to any particular trapping level (E_C-E_T) is a function

*Hewlett-Packard, Palo Alto, CA.
**Princeton Applied Research, Princeton, NJ.
14. G. L. Miller et al., "A Correlation Method for Semiconductor Transient Signal Measurements," J. Appl. Phys. 46, 2638 (1975).

of the absolute temperature T. A correlation technique is used to detect the trapping levels by comparing the measured transient signal as a function of temperature to a standard exponential decay function generated by the computer for a selected time constant. The correlator output increases as the time constant of the measured transient signal gets closer to the selected time constant and decreases as the time constant of the measured transient signal becomes shorter or longer than the selected time constant. Thus the presence of traps at several energy levels is indicated by a series of peaks in the correlator-output as a function of temperature. A rough estimate of the trap energy levels can be obtained from the temperature at the peak. However, a more precise determination requires a set of measurements of τ over a range of temperature so that a plot of log τ vs 1/T can be made.

In this work, a computer program has been written to control the whole system and carry out the necessary calculations. The associated temperature measurement and control unit has also been completed. Initial experiments were carried out on an Au-doped Si p-n junction to calibrate the DLTS system and compare the results with those obtained from other systems. The correlation with published results was excellent.

DLTS measurements were made on Schottky-barrier diodes deposited on several ion-implanted and epitaxial GaAs wafers. Figures 39 and 40 show the DLTS spectrum of ion-implanted GaAs wafers A57-B1 and A49A, respectively. In the A57-B1 wafer, 0.8- and 0.6-eV trap levels were detected, while 0.8-, 0.6-, 0.45-, and 0.3-eV trap levels were found in wafer A49A. Trap levels at 0.6 and 0.45 eV have been reported by Hasegawa et al. [15,16]. Further study is required to identify the 0.8- and 0.3-eV trap levels.

Figures 41 and 42 show the DLTS correlator-output spectra of epitaxial GaAs wafers D-422 and D-457, respectively. Wafer D-457 has an undoped buffer layer between the n-layer and substrate while wafer D-422 has no buffer layer. It is interesting to note that the spectrum of D-422 shows the 0.6- and 0.45-eV trap levels, but D-457 (which has a buffer layer) shows only the 0.45-eV trap level. This might indicate that the absence of the 0.6-eV trap level in wafer

15. F. Hasegawa and A. Majerfeld, "Majority Carrier Traps in n- and p-type Epitaxial GaAs," Electron. Lett. 11, 286 (1975).
16. F. Hasegawa and A. Majerfeld, "Effect of Heat Treatment on the Nature of Traps in Epitaxial GaAs," Electron. Lett. 12, 52 (1976).

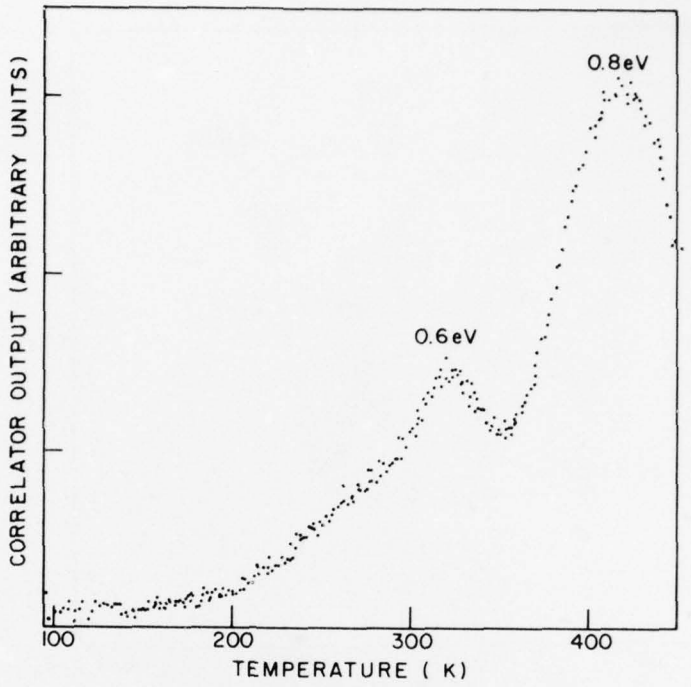

Figure 39. DLTS spectrum of ion-implanted sample A57-B1.

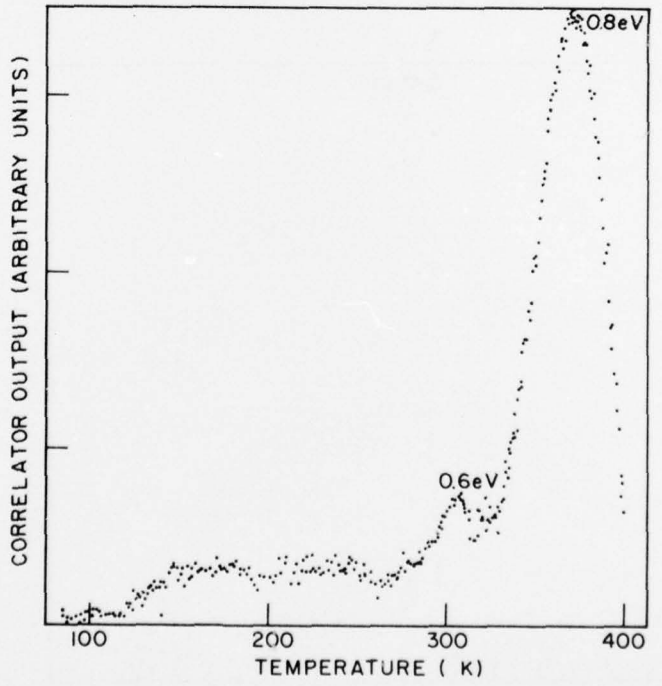

Figure 40. DLTS spectrum of ion-implanted and thermally annealed sample A49A. Vertical axis normalized so that peak amplitude is proportional to trap density. Distinct traps at 0.6 and 0.8 eV, possibly traps at 0.3 and 0.45 eV also.

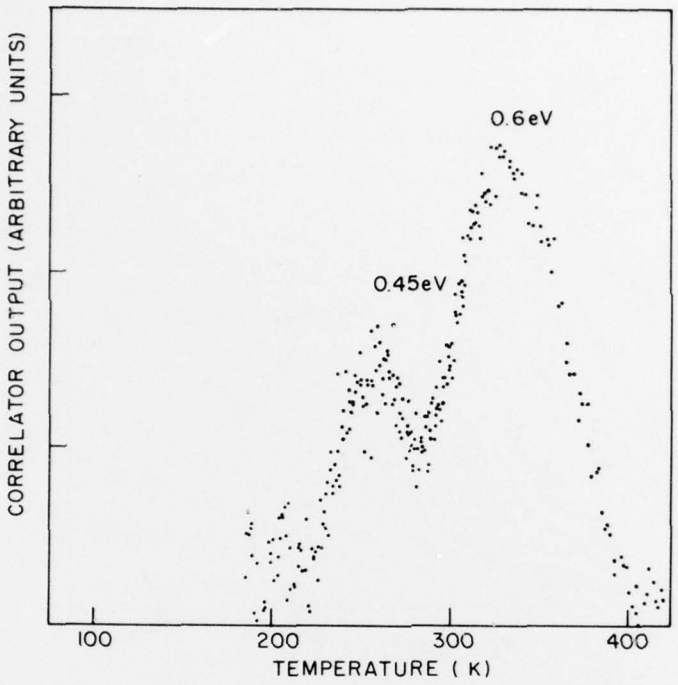

Figure 41. DLTS spectrum of epitaxial GaAs wafer (D-422). No buffer layer.

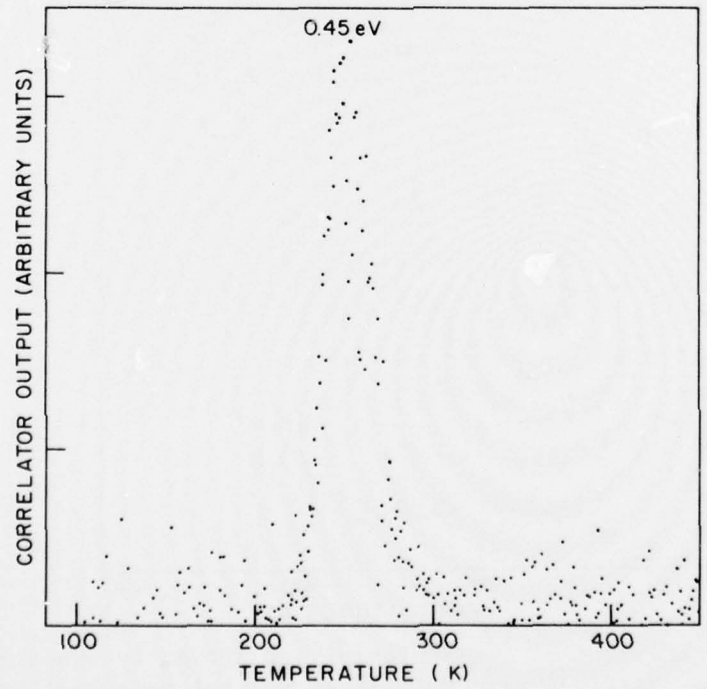

Figure 42. DLTS spectrum of epitaxial GaAs wafer (D-457) with undoped buffer layer.

D-457 has something to do with the presence of the buffer layer. This example demonstrates the utility of trap measurements. We will carry out a more detailed study of traps in ion-implanted GaAs to aid in the development of annealing techniques. The effect of various epitaxial high-resistivity buffer layers on epitaxy and ion implantation will be studied.

The key feature of our measurement system is that the capacitance transient is acquired, digitized, and stored for data manipulation. This provides a degree of flexibility that cannot be realized with analog schemes.

REFERENCES

1. S. T. Jolly et al., Epitaxial Growth of Semi-Insulating GaAs, Annual Report, Contract N00014-77-C-0542, DARPA Order No. 3461 Basic Program Code 7D10, March 1978.
2. G. B. Stringfellow and G. Horn, "Hydride VPE Growth of GaAs for FETs," J. Electrochem. Soc. 124, 1806 (1977).
3. H. M. Cox and J. V. DiLorenco, "Characteristics of an $AsCl_3/Ga/H_2$ Two-Bubbler GaAs CVD System for MESFET Applications," Proc. Sixth Int. Symp. GaAs and Related Compounds; Inst. Phys. Conf. Series, No. 33b, London, 1977, pp. 11-22.
4. J. K. Kennedy et al., "Effect of H_2 Carrier Gas Flow Rate on the Electrical Properties of GaAs in a Hydride System," J. Cryst. Growth 24/25, 233 (1974).
5. E. I. Shtyrkov, I. B. Khaibullin, M. M. Zaripov, M. F. Galyatudinov, and R. M. Bayazitov, "Local Annealing of Implantation Doped Semiconductor Layers," Sov. Phys. Semicond. 9, 1309 (1976).
6. S. U. Compisano, I. Catalano, G. Foti, E. Rimini, F. Eisen, and M. A. Nicolet, "Laser Reordering of Implanted Amorphous Layers in GaAs," Solid-State Electron. 21, 485 (1978).
7. R. T. Young, C. W. White, G. J. Clark, J. Narayan, W. H. Christie, M. Murakami, P. W. King, and S. D. Karmer, "Laser Annealing of Boron-Implanted Silicon," Appl. Phys. Lett. 32, 139 (1978).
8. S. G. Liu, C. P. Wu, and C. W. Magee, "Annealing of Ion-Implanted GaAs with Nd:Glass Laser," presented at the Symp. on Laser-Solid Interaction and Laser Processing (SLSILP) held in Boston, MA, Nov. 28-Dec. 1, 1978. Proceedings in press.
9. B. J. Sealy, M. H. Badawi, S. S. Kular, and K. G. Stephens, "Electrical Properties of Laser-Annealed Donor-Implanted GaAs," Electron. Lett. 14, 720 (1978).
10. A. Gat and J. F. Gibbons, "A Laser-Scanning Apparatus for Annealing of Ion-Implantation Damage in Semiconductors," Appl. Phys. Lett. 32, 142 (1978).

11. W. L. Brown, J. A. Gdovchenko, K. A. Jackson, L. C. Kimerling, H. J. Leamy, G. L. Miller, J. M. Poate, J. W. Rodgers, G. A. Rozgonyi, T. T. Sheng, T. N. C. Venkatesan, and G. K. Celler, "Laser-Annealing of Ion-Implanted Semiconductors," Proc. on Rapid Solidification Proc. - Principles and Technologies, Reston, VA, Nov. 1977.

12. R. Tsu, J. E. Baglin, G. J. Lasher, and J. C. Tsang, "Laser-Induced Damage and Recrystallization of Ion-Implanted GaAs by Frequency-Doubled Nd:Yag Laser," Presented at SLSILP (c.f. Ref. 8).

13. D. V. Lang, "Deep-Level Transient Spectroscopy: A New Method to Characterize Traps in Semiconductors," J. Appl. Phys. 45, 3023 (1974).

14. G. L. Miller et al., "A Correlation Method for Semiconductor Transient Signal Measurements," J. Appl. Phys. 46, 2638 (1975).

15. F. Hasegawa and A. Majerfeld, "Majority Carrier Traps in n- and p-type Epitaxial GaAs," Electron. Lett. 11, 286 (1975).

16. F. Hasegawa and A. Majerfeld, "Effect of Heat Treatment on the Nature of Traps in Epitaxial GaAs," Electron. Lett. 12, 52 (1976).

DISTRIBUTION LIST

Program Management
DARPA
Architect Building
1400 Wilson Blvd
Arlington, VA 22209 (2)

Code 427
Office of Naval Research
Arlington, VA 22217
(3)

Naval Research Laboratory
4555 Overlook Ave, SW
Washington, DC 20375
Attn: Code 5220 (1)

Naval Research Laboratory
4555 Overlook Ave, SW
Washington, DC 20375
Attn: Code 5270 (1)

Defense Documentation Center
Building 5
Cameron Station
Alexandria, VA 22314 (12)

ONR Boston
495 Summer Street
Boston, MA 02210
(1)

TACTEC
Battelle Memorial Institute
505 King Avenue
Columbus, OH 43201
(1)

Dr. Y.S. Park
AFAL/DHR
Building 450
Wright-Patterson AFB, OH 45433
(1)

ERADCOM
DELET-M
Fort Monmouth, NJ 07703
(1)

Texas Instruments
MS 105
PO Box 5936
Dallas, TX 75222
(1)

Dr. R.M. Malbon
Avantek, Inc
3175 Bowers Ave
Santa Clara, CA 95051 (1)

Dr. R. Bell, K101
Varian Associates
611 Hansen Way
Palo Alto, CA 94304
(1)

Mr. R. Bierig
Raytheon Company
28 Seyon Street
Walthon, MA 02154
(1)

Dr. H.C. Nathanson
Westinghouse R&D Center
Beulah Road
Pittsburgh, PA 15235
(1)

Dr. F. Blum
Rockwell International Ctr
PO Box 1085
Thousand Oaks, CA 91360
(1)

Mr. G.J. Gilbert
MSC
100 Schoolhouse Road
Somerset, NJ 08873
(1)

Mr. C. Krumn
Hughes Research Laboratory
3011 Malibu Canyon Road
Malibu, CA 90265
(1)

Mr. Hunter Chilton
RADC/OCTE
Griffiss AFB, NY 13441
(1)

Mr. Lothar Wandinger
ECOM/AMSEL/TL/IJ
Fort Monmouth, NJ 07703
(1)

Colonel Paul Mosteller
AFOSR/NE, Bldg 410
Bolling AFB, DC 20375
(1)

Dr. Harry Wieder
Naval Ocean Systems Center
Code 922
271 Catalina Blvd
San Diego, CA 92152 (1)

Dr. William Lindley
MIT/Lincoln Laboratory
E124A, PO Box 73
Lexington, MA 02173 (1)

Dr. Sven Roosild
AFCRL/LOD
Hanscom AFB, MA 01731
(1)

Mr. John Kennedy
AFCRL/LOP
Hanscom AFB, MA 01731
(1)

Mr. Don Reynolds
AFAL/DHR
Wright-Patterson AFB, OH 45433
(1)

Mr. John Carroll
RADC/RBRP
Griffiss AFB, NY 13441
(1)

Dr. Robert Thomas
RADC/RBRM
Griffiss AFB, NY 13441
(1)